Using machine learning techniques for predicting autogenous shrinkage of concrete incorporating superabsorbent polymers and supplementary cementitious materials

Benoit Hilloulin, van Quan Tran

Using machine learning techniques for predicting autogenous shrinkage of concrete incorporating superabsorbent polymers and supplementary cementitious materials

Benoît Hilloulin[1],Van Quan Tran[2,] *

[1] Institut de Recherche en Génie Civil et Mécanique (GeM), UMR-CNRS 6183, Ecole Centrale de Nantes, 1 rue de la Noë, 44321 Nantes, France – e-mail: benoit.hilloulin@ec-nantes.fr

[2]University of Transport Technology, Hanoi 100000, Vietnam

*Corresponding author: quantv@utt.edu.vn

Highlights

- Experimental data about the influence of SAP on shrinkage were collected
- Machine learning models predict shrinkage/expansion of concrete with SAP and SCM
- XGBoost is the most precise machine learning model for shrinkage prediction
- SHAP and partial difference plots quantify inputs' influence on model results

Abstract

Superabsorbent polymers (SAP) are a very effective means of decreasing high-performance and ultra-high performance concrete autogenous shrinkage. However, their efficiency can hardly be predictable because of various parameters: SAP properties, supplementary cementitious materials (SCM) nature, and cement replacement ratios. This study provides a machine learning approach for predicting shrinkage/expansion in cementitious materials incorporating SAP and SCM. A dedicated database is built, and four machine learning models are compared. Extreme Gradient Boosting (XGBoost) model exhibited the highest accuracy. SHapley Additive exPlanations (SHAP) allowed the identification of the most influential inputs, and partial dependence plots provided quantitative information about their relative influence.

Keywords: Concrete; shrinkage; Superabsorbent polymer (SAP); Machine Learning; Gradient Boosting.

1. Introduction

Concrete is the most consumed human-made material on Earth due to its cost, strength, and local availability of its components. A wide range of cementitious materials has been developed: from lightweight concrete to self-compacting concrete and high-performance or ultra-high performance concrete. These materials, carefully selected depending on the required mechanical properties and necessary durability depending on their prospective environmental exposure, can be subjected to several types of degradation, one of the most prejudicial being cracking. Cracking can appear due to several reasons during the lifetime of a structure. One of the major causes of cracking during the first weeks after casting is restrained shrinkage which appears when a structural element tends to shrink but cannot shrink due to surrounding elements [1–3].

Several shrinkage mechanisms generally add up and produce total shrinkage: chemical shrinkage, plastic shrinkage, autogenous shrinkage, drying shrinkage, thermal shrinkage, and carbonation shrinkage. Within the first days after casting, autogenous shrinkage has been reported as the major shrinkage mechanism in high-strength concrete (HPC) and ultra-high performance concrete (UHPC). These cementitious materials, known for their good mechanical properties and durability, are formulated with limited or small water-to-cement ratios (w/c), generally below 0.4 for HPC and 0.3 for UHPC. Self-desiccation develops quickly within the capillary pores as relative humidity drops, creating capillary depressions within the skeleton because of the small amount of water available for cement hydration. Due to these microscopic evolutions, autogenous shrinkage, defined as the external macroscopic volume reduction that occurs under isothermal/sealed conditions, is measured, and cracking might occur within the first days/weeks [4,5].

The initial concrete composition greatly influences autogenous shrinkage, and the actual development of cementitious materials, incorporating vast amounts of supplementary cementitious materials, motivates a deep understanding of their relative role in shrinkage [6,7]. First, besides the water-to-cement or water-to-binder (w/b) ratios, it was found that cement fineness generates more autogenous shrinkage, while the higher the aggregate-to-binder ratio, the smaller the autogenous shrinkage due to the restraining effect of aggregates [8]. Then, during the last decades, it was found that autogenous shrinkage is significantly increased by the presence of silica fume in HPC and UHPC, leading to careful monitoring of autogenous shrinkage in such mixes [9,10]. The addition of 5% or 10% silica fume was found to increase significantly autogenous shrinkage, and three main mechanisms are generally used to explain this increase: i) the refined pore structure, ii)

the increased formation of CSH with a porous structure due to portlandite consumption and iii) the acceleration of hydration and water adsorption around silica fume particles [6]. To a smaller extent, though this question is still under debate, slag was also found to negatively influence shrinkage in some cases with 30%-50% replacement ratios [11,12], while it was found to create a relative expansion in other studies and specifically in some UHPC mixes. The negative influence of slag on autogenous shrinkage has been related to the increased chemical shrinkage due to slag, chemical shrinkage being a driving force of autogenous shrinkage. At the opposite, fly ash was found to reduce shrinkage for replacement ratios between 15% and 60% because of the slower hydration reaction of mixes incorporating fly ash, but its effect might be limited for smaller replacement ratios [13,14]. Similarly, calcined clay was found to decrease autogenous shrinkage during the first weeks but can increase long-term autogenous shrinkage [15–17], and filler is generally reported to decrease shrinkage, acting as a small aggregate mitigating the shrinkage of the cement paste [18,19]. Due to these adverse effects, the global autogenous shrinkage behavior of complex concrete formulations is worth being investigated, especially in the case of slag and limestone filler blends [20], limestone calcined clay cement (LC3) [21], or eco-friendly ultra-high performance concrete [22,23].

Autogenous shrinkage can be mitigated using specific additives in concrete. Several additives have been employed, from natural components to engineered materials [24,25]. First, it was found that some lightweight aggregates can reduce shrinkage due to their intrinsic porosity leading to the gradual release of water during the first days after casting. For example, pumice has been reported to reduce shrinkage considerably [26]. Novel materials have been designed to mitigate shrinkage and subsequent cracking during the last decades. Superabsorbent polymers, which are polymer particles able to store extra water during mixing and restore their water during the first days [27], have also been successfully employed to mitigate concrete shrinkage [28–31] and are further being developed for some years in order to optimize their water absorption capacity and release rate in the high pH concrete matrix. When incorporated in the concrete mix by around 0.2 to 0.6% of cement mass, SAP have been proved to be an effective solution in mitigating autogenous shrinkage, drying shrinkage [32], and stress development [33], although some later deformations might be observed when SAP become empty. The efficiency of SAP, which intrinsically relies on their nature the initial cross-linking and the nature of the chemical components [34], can be assessed before concrete mixing by performing absorption tests on the SAP such as the ‘tea bag method’ and the ‘filtration method’ [35–37]. Though precise chemical information about SAP

composition had not been reported systematically [31], SAP with various initial composition and absorption characteristics (either ‘releasing’ or ‘retentive’) have been found effective in reducing autogenous shrinkage [38]. SAP diameter, which was initially assumed to play a role in the shrinkage mitigation capacity, is a less important parameter as long as SAP particles are evenly distributed within the cementitious matrix [39]. Besides their interest concerning autogenous shrinkage mitigation, SAP are also helpful in drying and plastic shrinkage mitigation, enhancing self-healing, and increasing freeze-thaw resistance [31].

For the reasons above, a precise understanding of the effect of SAP on the autogenous shrinkage of high-performance and ultra-high performance concrete mixes incorporating supplementary cementitious materials is necessary to anticipate the harmful consequences of cracking in modern concrete. Machine learning predictions would help design such complex materials. Indeed, artificial intelligence techniques have been successfully applied to several Civil Engineering problems such as concrete strength prediction [40,41], creep prediction [42–44], crack assessment in structures [45] or durability and microstructural properties such as surface chloride concentration [46] and and mechanical properties of stabilized soil [47,48]. Among the various techniques developed, ensemble machine learning algorithms applied to datasets with hundreds of data points have proved a good accuracy and robustness against overfitting risk, often associated to conventional techniques and neural networks. Some machine learning models were successfully applied to autogenous or drying shrinkage modeling, but most of them [42,49–51] did not consider SCM, and, to date, no model has been proposed for the shrinkage or swelling prediction of cementitious materials incorporating SAP.

This study provides an insight into the potential of machine learning models, based on conventional or ensemble techniques, to predict the autogenous shrinkage / swelling properties of cementitious materials, incorporating supplementary cementitious materials. A database has been specifically built based on the NU database and the available literature. The theory and procedure associated with the models are briefly presented in the manuscript. Then, the results of the models are discussed, and the best model candidate is further examined using SHapley Additive exPlanation (SHAP) theory to understand the most influential features. Finally, partial difference plots are used to quantitatively assess the influence of the features on the shrinkage / swelling predictions.

2. Database description and analysis

Observations of autogenous shrinkage were selected from NU database [52] (187 observations) and published studies about autogenous shrinkage of low water-to-cement ratio cement paste, mortar or concrete samples incorporating SCM [5,8,10,11,13–15,17,20,21,53–68,68–74] and / or SAP [28,29,33,39,75–87] (142 and 108 values respectively). In total, 437 autogenous shrinkage curves were used to interpolate shrinkage (or swelling) at various ages, e.g., 1d, 2d, 7d, 14d, and 28d. Based on these interpolations, 1889 shrinkage data points were generated, ranging between 1166 με (swelling with SAP) and -3818.9 με (shrinkage of a low w/c cement paste). Fourteen parameters have been selected as model inputs: water-cement ratio, water-binder ratio, aggregate-cement ratio, cement content (kg/m^3), silica fume content (% cement mass), fly ash content (% cement mass), slag content (% cement mass), calcined clay content (% cement mass) (denoted as metakaolin), filler content (kg/m^3), amount of superplasticizer (% cement mass), SAP content (% cement mass), SAP size (μm), SAP water uptake (g / g of SAP in cement slurry) and time since the beginning of shrinkage measurements (days). Compressive strength and Young's modulus were deliberately not used as inputs to build a model using only formulation inputs without any need to perform additional experiments. Shrinkage (or swelling) value at a given age was the targeted value. Moreover, as NU database does not include the shrinkage measurement method (among inductive sensors, laser sensors, hydrostatic scales; forming cuboidal samples in foil, corrugated PP tubes, buoyancy method), the shrinkage measurement methodology was not accounted for in the database.

Details about the database composition are given in Table 1. Median values of 0.35 and 0.30 were obtained for water-to-binder, and water-to-cement ratios resp., which corresponds to average experimental values reported in autogenous shrinkage studies. A median cement content of around 500 kg/m^3 was obtained, which is consistent for this type of study. Histograms of the input and output values are given in Fig. 1. As illustrated in Fig. 1 k), SAP contents of 0.2, 0.4, and 0.6 % cement mass were mostly used in the studies selected to build the database.

Histograms of the input data are given in Fig. 1. Correlations between the variables were calculated prior to machine learning algorithms application. The correlation matrix is given in Fig. 2. As expected, the first four parameters (water-cement ratio, water-binder ratio, aggregate-cement ratio, cement content) were particularly correlated and relatively well correlated with autogenous shrinkage / swelling values. Interestingly, the three variables concerning SAP were found to be correlated too, highlighting common practices when using SAP such as adapting the SAP content

depending on SAP swelling capacity [88] and selecting SAP size depending on the application, for example, autogenous shrinkage reduction, leading to a correlation with SAP swelling capacity.

Table 1. Description of the database used in this study

	No	Unit	Count	Mean	Median	Min	Max	$Q_{25\%}$	$Q_{75\%}$	Std	Skw
W/C	1	-	1889	0.40	0.35	0.17	1.60	0.3	0.44	0.17	3.36
W/B	2	-	1889	0.33	0.3	0.157	0.86	0.266	0.374	0.11	1.49
A/C	3	-	1889	2.83	3.28	0	11.56	1.24	4.02	2.02	0.33
Cement	4	kg/m^3	1889	637.41	498	167.4	1762.00	418	700	364.99	1.53
Silica fume	5	(*)	1889	4.80	0	0	50.00	0	10	8.44	2.32
Fly ash	6	(*)	1889	5.13	0	0	100.00	0	0	14.32	3.21
Slag	7	(*)	1889	8.05	0	0	400.00	0	0	36.71	7.28
Metakaolin	8	(*)	1889	0.70	0	0	57.40	0	0	4.85	9.46
Filler	9	(*)	1889	4.51	0	0	125.00	0	0	13.83	3.98
Superplasticizer	10	(*)	1889	1.39	0.8	0	11.82	0	1.8	1.98	2.49
SAP	11	(*)	1889	0.06	0	0	0.92	0	0	0.16	2.68
SAP size	12	µm	1889	43.01	0	0	645.00	0	0	107.15	3.33
SAP water uptake	13	(**)	1889	4.51	0	0	61.00	0	0	10.89	3.32
Time	14	days	1889	9.06	7	1	28.00	2	14	9.40	1.08
Shrinkage/Swelling		µε	1889	-280.93	-136.6	-3818.9	1166.70	-382.2	-26.4	491.77	-2.69

(*) % cement mass; (**) g/g of SAP; Skw=Skewness; Std=Standard deviation;

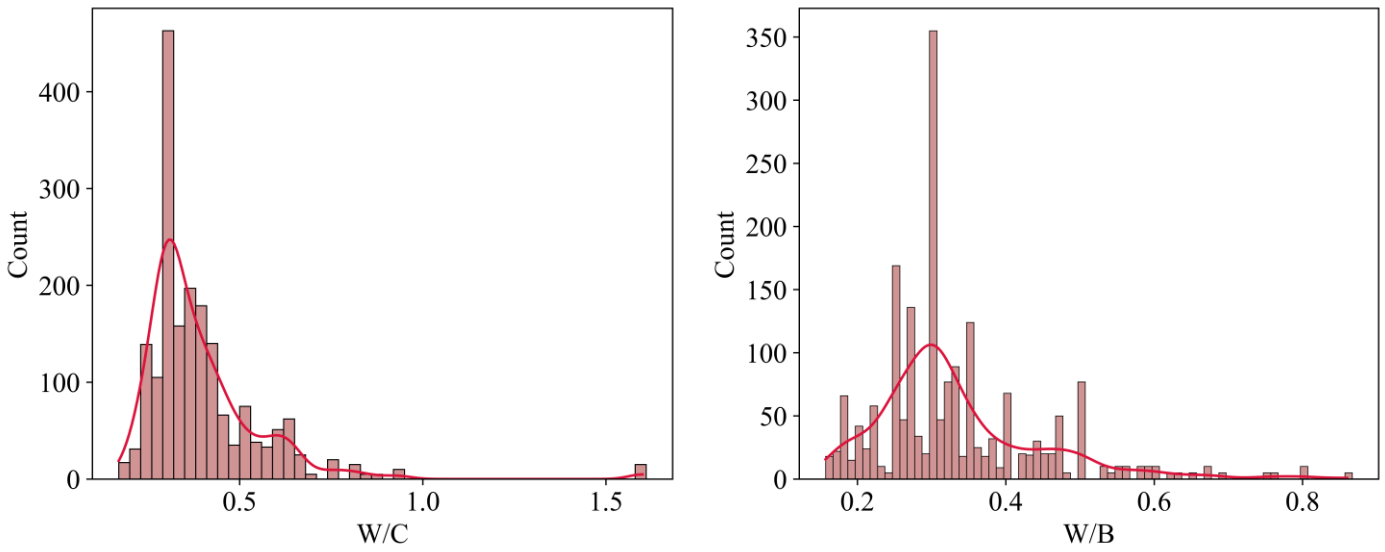

(a) (b)

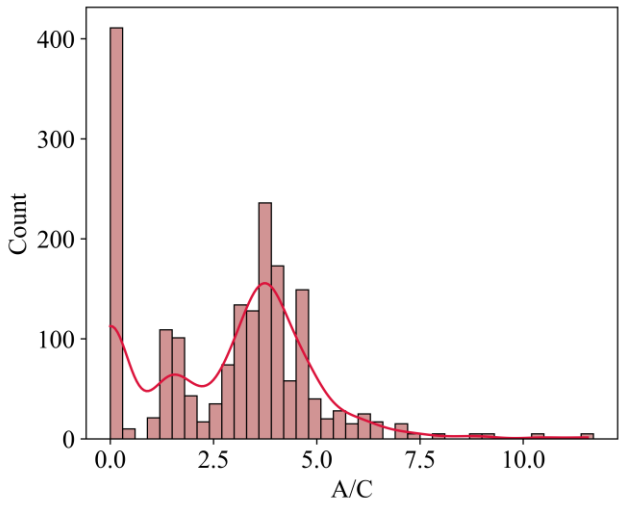
Count
A/C
0.0
2.5
5.0
7.5
10.0
0
100
200
300
400

(c)

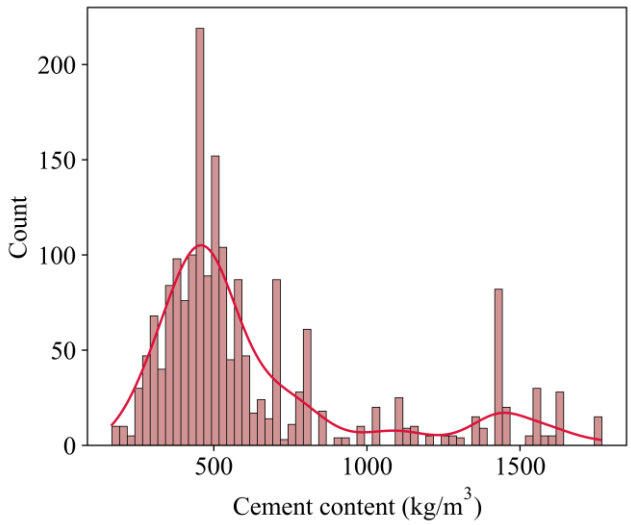
Count
Cement content (kg/m3)
0
500
1000
1500
50
100
150
200

(d)

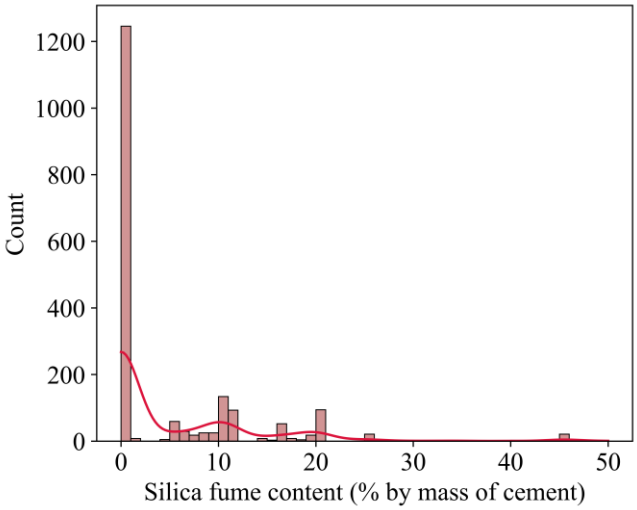
Count
Silica fume content (% by mass of cement)
0
10
20
30
40
50
200
400
600
800
1000
1200

(e)

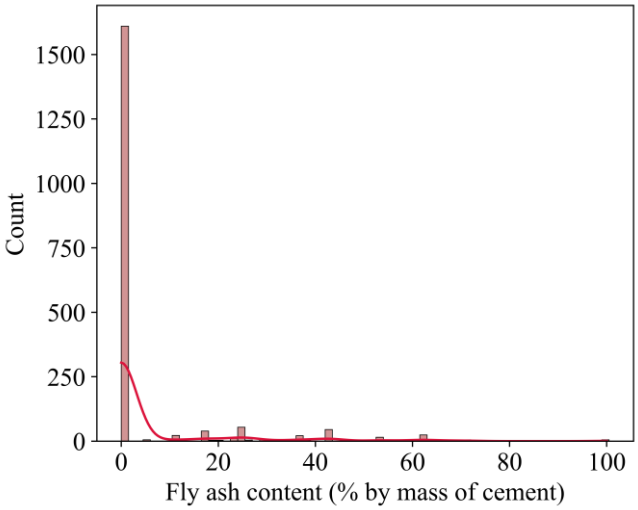
Count
Fly ash content (% by mass of cement)
0
20
40
60
80
100
250
500
750
1000
1250
1500

(f)

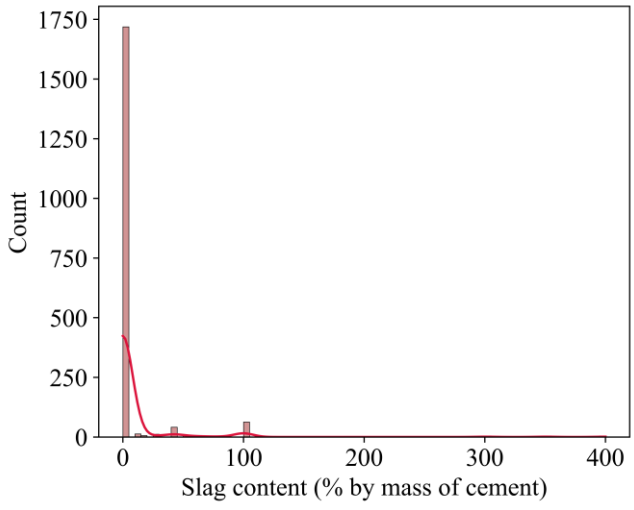
Count
Slag content (% by mass of cement)
0
100
200
300
400
250
500
750
1000
1250
1500
1750

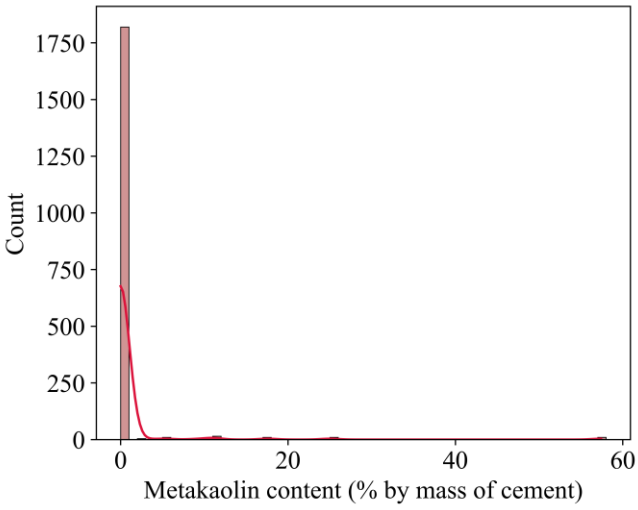
Count
Metakaolin content (% by mass of cement)
0
20
40
60
250
500
750
1000
1250
1500
1750

(g)

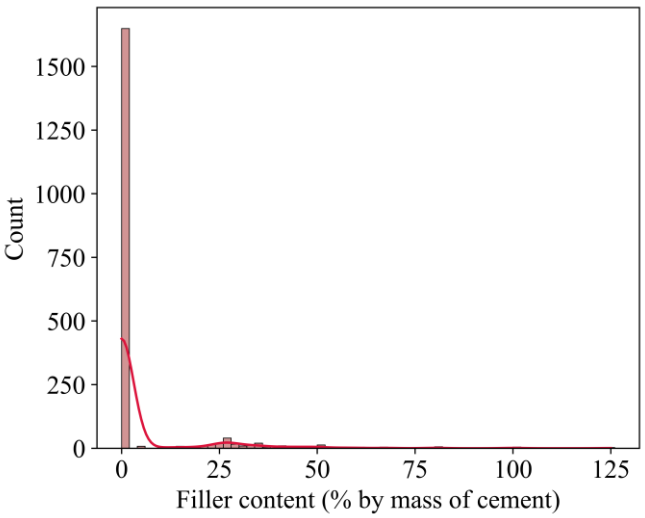
Count
1500
1250
1000
750
500
250
0
0
25
50
75
100
125
Filler content (% by mass of cement)

(h)

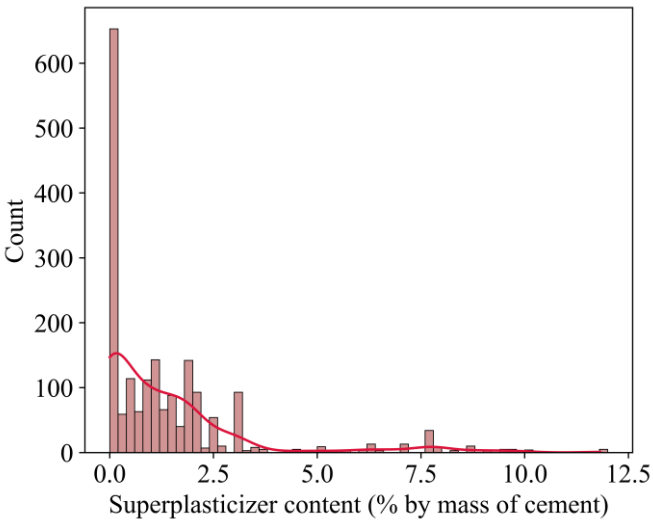
Count
600
500
400
300
200
100
0
0.0
2.5
5.0
7.5
10.0
12.5
Superplasticizer content (% by mass of cement)

(i)

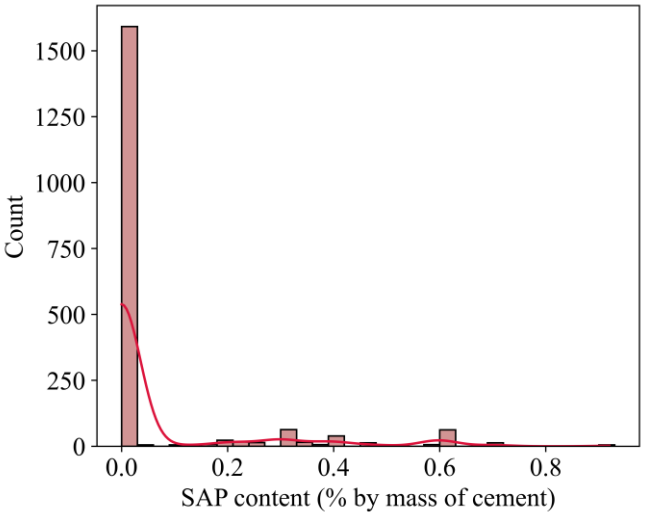
Count
1500
1250
1000
750
500
250
0
0.0
0.2
0.4
0.6
0.8
SAP content (% by mass of cement)

(j)

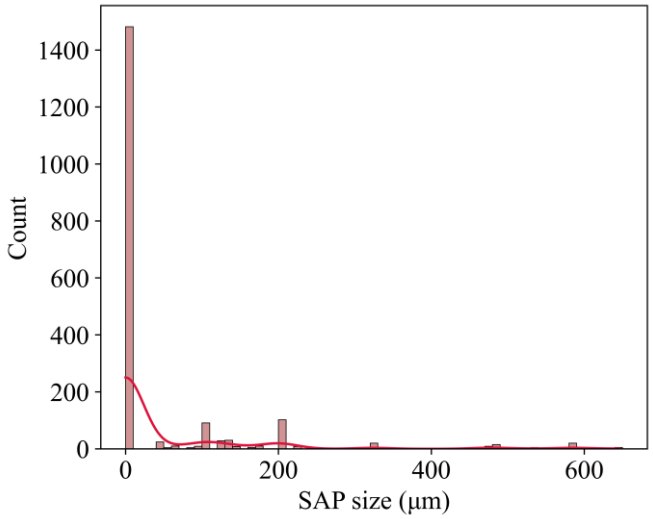
Count
1400
1200
1000
800
600
400
200
0
0
200
400
600
SAP size (μm)

(k)

(l)

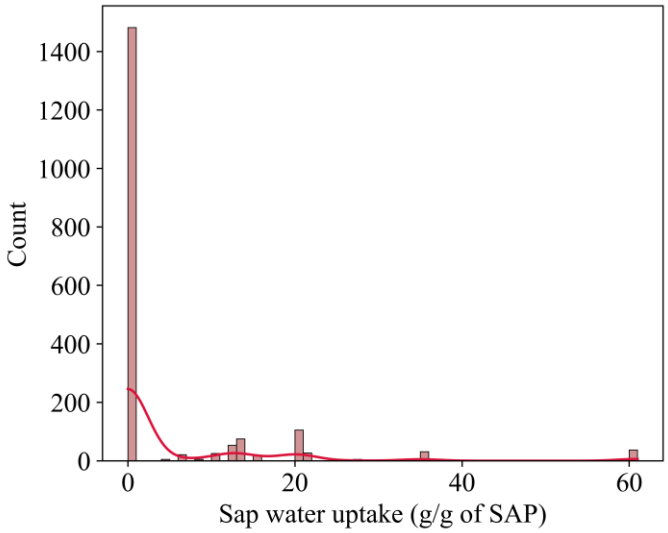

(m)

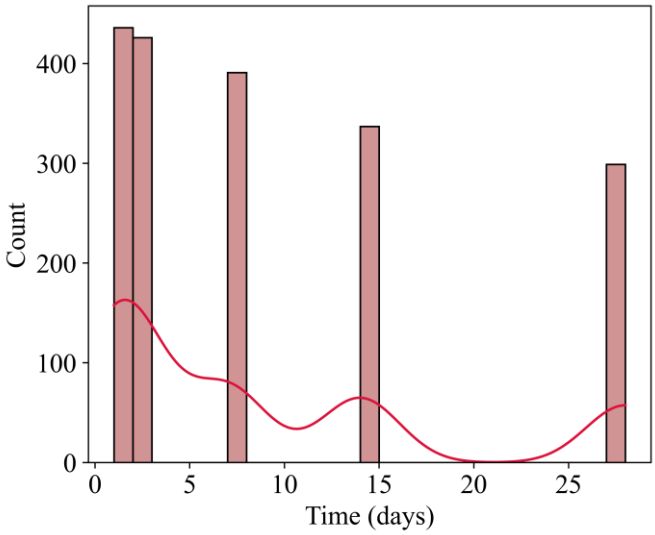

(n)

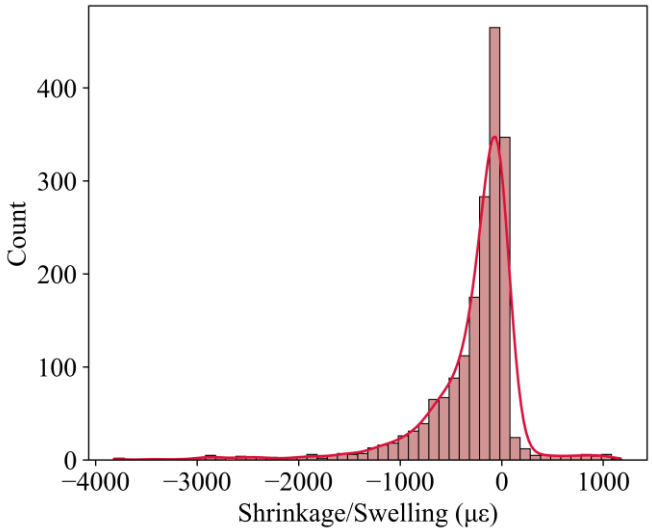

(o)

160 **Fig. 1.** Data distribution of each input variable and the output variable (shrinkage/swelling).

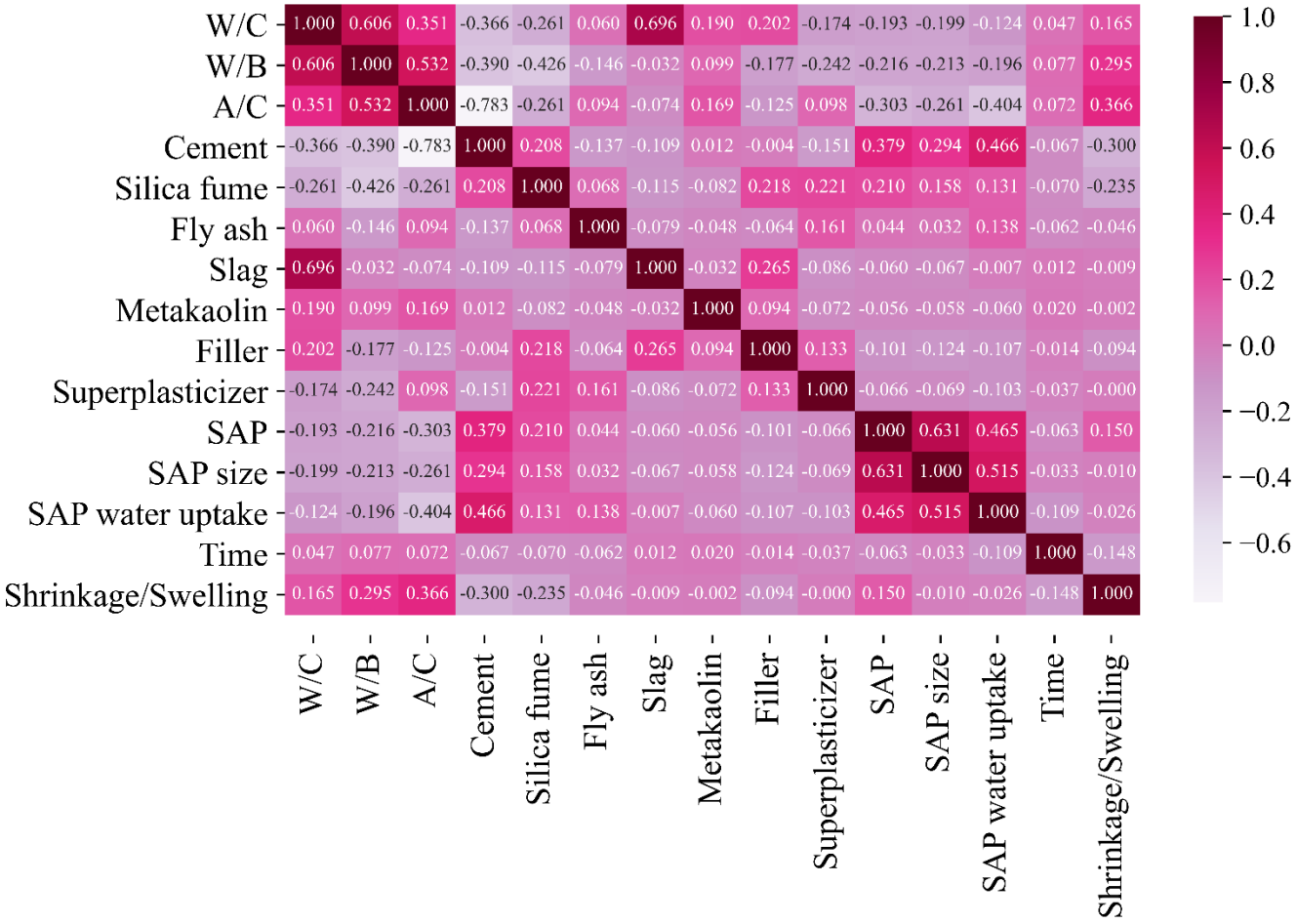

Fig. 2. Correlation matrix of the input and output variables

3. Machine Learning Methods

In this study, four kinds of state-of-the-art Machine Learning (ML) models have been used, three of them being ensemble models, generally the best models for medium tabular data encountered in Civil Engineering problems. The four ML algorithms: K-Nearest Neighbors (KNN), Random Forest (RF), Gradient Boosting (GB), and Extreme Gradient Boosting (XGB), are briefly presented in this section. As the performances of ML models depend strongly on their hyperparameters, the default hyperparameters used in Sklearn were selected, which helps reduce the time of building ML model. The Monte Carlo simulation (MCS) is chosen as a validation technique for evaluating the performance of ML models. The MCS and k-fold cross-validation are two common validation techniques. However, the MCS can give the results with higher confidence and lower variance than the k-fold cross-validation technique.

3.1. K-Nearest Neighbors (KNN)

The k-nearest neighbors' algorithm (k-NN) is a non-parametric classification method invented in 1951 by Fix and Hodges [90] and later extended by Altman [91]. The input in both cases consists of the k closest training examples in a data collection. The result of k-NN regression is the object's property value. This value is the mean of the values of the k closest neighbors. A good strategy is to apply weights to the contributions of the neighbors, such that closer neighbors contribute more to the average than the neighbors who are farther away. Neighbors-based regression is a sort of lazy learning in that it does not seek to build a generic internal model and instead just saves instances of the training data [92]. As an average or local linear approximation, the regression result is obtained from the k-nearest neighbors of each point. This technique is easy to construct, resistant to noisy training data, and effective with huge amounts of training data. However, the value of k must be determined, and the calculation cost is high since it must compute the distance of each instance to all of the training examples.

3.2. Random Forest (RF)

Random forest (RF) is an ensemble learning technique used for classification, regression, and other applications. The RF method incorporates two powerful ML approaches, bootstrap aggregation [93] and random subspace [94]. Bagging generates n bootstrap sets by sampling with replacement N training instances from the training set. The number of bootstrap samples and features is arbitrary and is fewer than the original training set. Then, as illustrated in Fig. 3, each bootstrap set is generated as a decision tree (e). A decision tree identifies a bootstrap set by examining its properties at each node. Each node checks a specific property, with the tree's leaves reflecting the result labels. Moving down a certain tree branch evaluates specific properties at each node to arrive at an output label. The final result combines the outputs of all leaves [95]. The RF prediction output may be written as follows:

$$Y = \frac{1}{n_{trees}} \sum_{i=1}^{n_{trees}} Y_i(x) \quad (1)$$

Where Y is the average output of a total number of n_{trees}; $Y_i(x)$the single prediction of a tree for an input vector x.

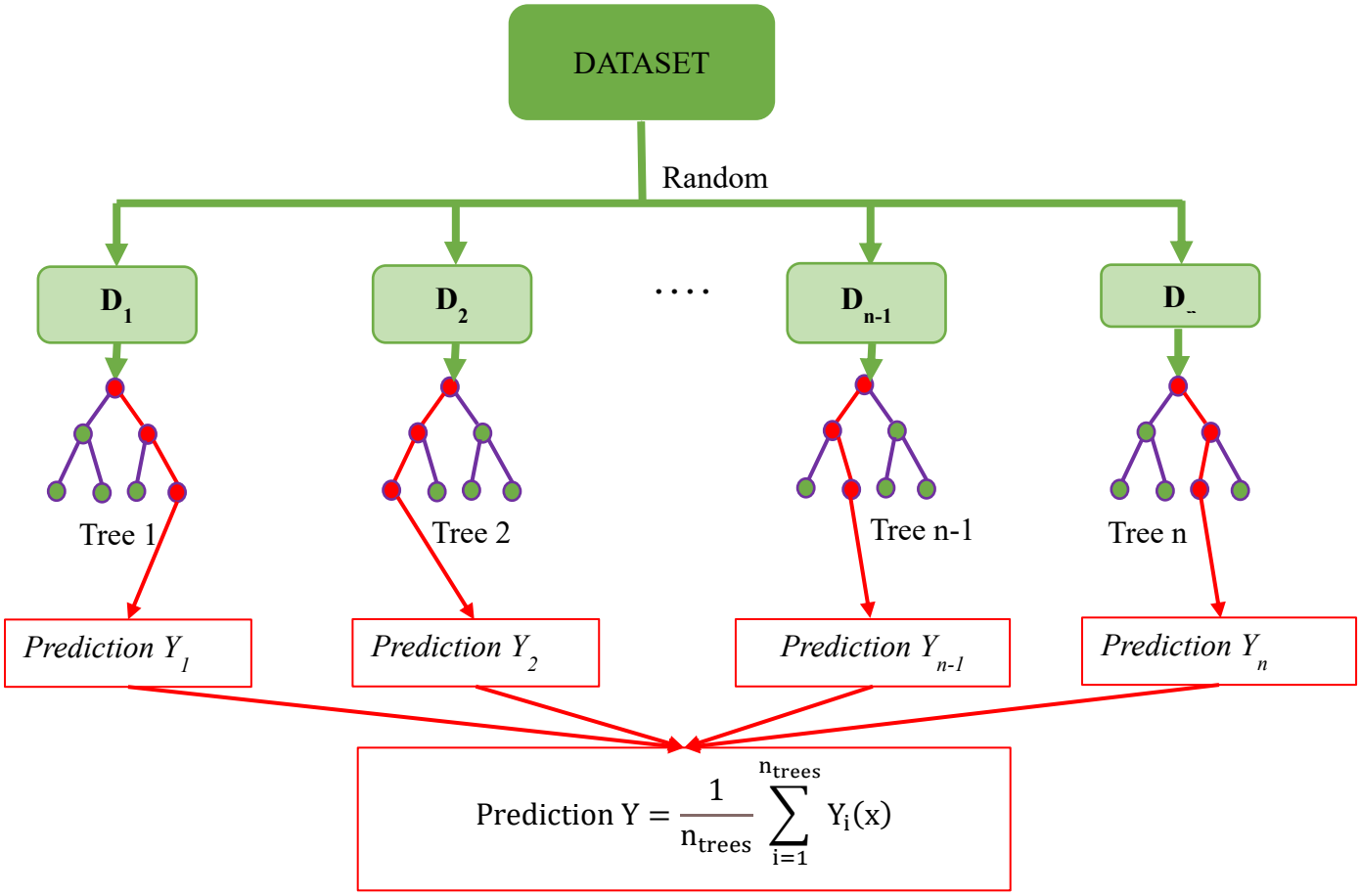

Fig 3. Schematic view of Random Forest

3.3. Gradient Boosting (GB)

Gradient boosting algorithm (GB), like random forest, is an ensemble approach that belongs to a family of techniques that use many classifications or regression trees in its algorithm to provide a reliable and desired output. In GB, classification or regression trees, also known as base learners, are built consecutively to increase the algorithm's performance. GB was originally designed for classification problems exclusively, though Friedman expanded it to regression challenges [96]. During each iteration, the GB algorithm considers the previously ensemble tree mistake and attempts to recover the error while predicting the next tree. As a result, the inaccuracy in future tree ensembles is constantly decreasing. Furthermore, GBM is based on the notion of boosting, in which numerous combinations of models with high bias and low variance are used to substantially reduce the high bias while preserving the low variance. This means that GBM combines numerous shallow trees to increase prediction performance. The shallow trees are learned using the same dataset as the deep trees. It is worth noting that the gain in prediction performance has endeared it

to many academics from other fields, including civil engineering [97,98].

3.4. Extreme Gradient Boosting (XGB)

The XGB model is a sophisticated tree boosting method [99]. It is an enhancement to Friedman's gradient boosting approach [96]. It predicts the outcome using a number of additive functions.

$$\overline{Y}^{k}{}_{i} = \overline{Y}^{(k-1)}{}_{i} + \alpha f_k \tag{2}$$

where $\overline{Y}_i$ is the predicted result for the i_{th} sample, and x_i is the vector of features; N is the number of estimators, and each estimator f_k (with k ranging from 1 to N) corresponds to an independent tree structure; Y_i^0 is the initial guess, which is the mean of the measured values in the training set; and α is the learning rate which helps to improve the model smoothly while adding new trees and avoid overfitting It is worth noting that overfitting is the primary problem with all ML models. The training procedure is carried out in an additive manner. According to Eq. 2, at the k_{th} step, a k_{th} estimator is added to the model, and the k_{th} expected result $\overline{Y}^{k}{}_{i}$ is determined by subtracting the predicted value at the previous stage $\overline{Y}^{(k-1)}{}_{i}$ from the estimation f_k of the extra k_{th} estimator. f_k is determined by the leaf weights discovered by minimizing the objective function of the k_{th} tree specified by:

$$objective = \lambda T + \sum_{j=1}^{T}\left[E_j \omega + \frac{1}{2}\left(F_j + \gamma\right)\omega_j^2 \right] \tag{3}$$

where T is the number of k_{th} tree leaves and x_j with j ranging from 1 to T are the leaf weights; λ and γ are regularization parameters that govern the tree structure's simplicity to minimize overfitting. The parameters E_j and F_j, which are the sums of the samples associated with the j_{th} leaf of the loss function's first and second gradients, respectively.

Starting with a single leaf, the k_{th} tree is built by separating the leaves. This technique is carried out by maximizing the gain parameter, which is described by:

$$gain = \frac{1}{2}\left[\frac{E^2{}_L}{F_L + \gamma} + \frac{E^2{}_R}{F_R + \gamma} - \frac{\left(E_L + E_R\right)^2}{F_L + F_R + \gamma} \right] - \lambda \tag{4}$$

After the splitting, E_L and F_L are linked with the left leaf, while E_R and F_R are associated with

the right leaf. If the gain parameter is greater than zero, the splitting is accepted. As a result, raising the regularization parameters λ and γ reduces the gain parameter, allowing the tree structure to remain simple by avoiding the complexity of leaf splitting. However, it will impair the model's ability to fit the training data.

3.5. Performance evaluation of models

The model performances were evaluated using the following three metric indexes: coefficient of determination (R^2), root mean square error (RMSE) and mean absolute error (MAE), whose formulations are given as follows:

$$R^2 = \frac{\sum_{j=1}^{N}(p_{0,j} - \overline{p_0})(p_{t,j} - \overline{p_t})}{\sqrt{\sum_{j=1}^{N}(p_{0,j} - \overline{p_0})^2 \sum_{j=1}^{N}(p_{t,j} - \overline{p_t})^2}} \quad (5)$$

$$\text{RMSE} = \sqrt{\frac{1}{N}\sum_{j=1}^{N}(p_{0,j} - p_{t,j})^2} \quad (6)$$

$$\text{MAE} = \frac{1}{N}\sum_{j=1}^{N}\left|p_{0,j} - p_{t,j}\right| \quad (7)$$

Where $p_{0,j}$ is the shrinkage/expansion value of i-th sample point in the database; $p_{t,j}$ is the prediction value made by machine learning models for i-th sample point; $\overline{p_0}$is the averaged experimental value of shrinkage / expansion and $\overline{p_t}$ is the mean predicted value. Both MAE and RMSE explicitly characterize the residual error at each sample point and can give an exact evaluation of the model performance. In comparison, R^2 normalizes the squared residual error with the variance of the database and produces dimensionless scores ranging from 0 to 1. Because RMSE is generally considered more intuitive as it is comparable to measured values and convenient for comparing the performance of different models, it has been adopted as the main metric index in the following analysis

3.6. Methodology flow chart

The methodology diagram reported in Fig. 4 displays the investigation's design. The concept is separated into three key steps: step (I) database preparation and description, step (II) selection of the best ML model with the highest performance, and step (III) Shrinkage/Swelling prediction and

sensitivity analysis. In step one, samples are collected from various literature studies, including input and output variables. The database used to predict the shrinkage/swelling of concrete has fourteen input variables: W/C, W/B, A/C, Cement content, Silica fume content, Fly ash content, Slag content, Metakaolin content, Filler content, Superplasticizer content, SAP content, SAP size, SAP water uptake and time. In step two, the database is randomly divided into 70% for training (1322 samples) and 30% for testing (567 samples).Four ML models comprised of algorithms such as KNN, RF, GB, and XGB are employed for training the ML model. The coefficient of determination R^2, Root Mean Square Error RMSE, and Mean Absolute Error MAE are used to evaluate ML performance. The Monte Carlo Simulation MCS is used to analyze the performance of four ML models in order to select the best ML model using the default hyperparameters. In the final step, the best ML model is used to predict the shrinkage/swelling of concrete and assess the effect of each factor on the shrinkage/swelling of concrete using Shapley Additive Explanations (SHAP) and partial dependency analysis, including Individual Conditional Expectation Plots (ICE) [100].

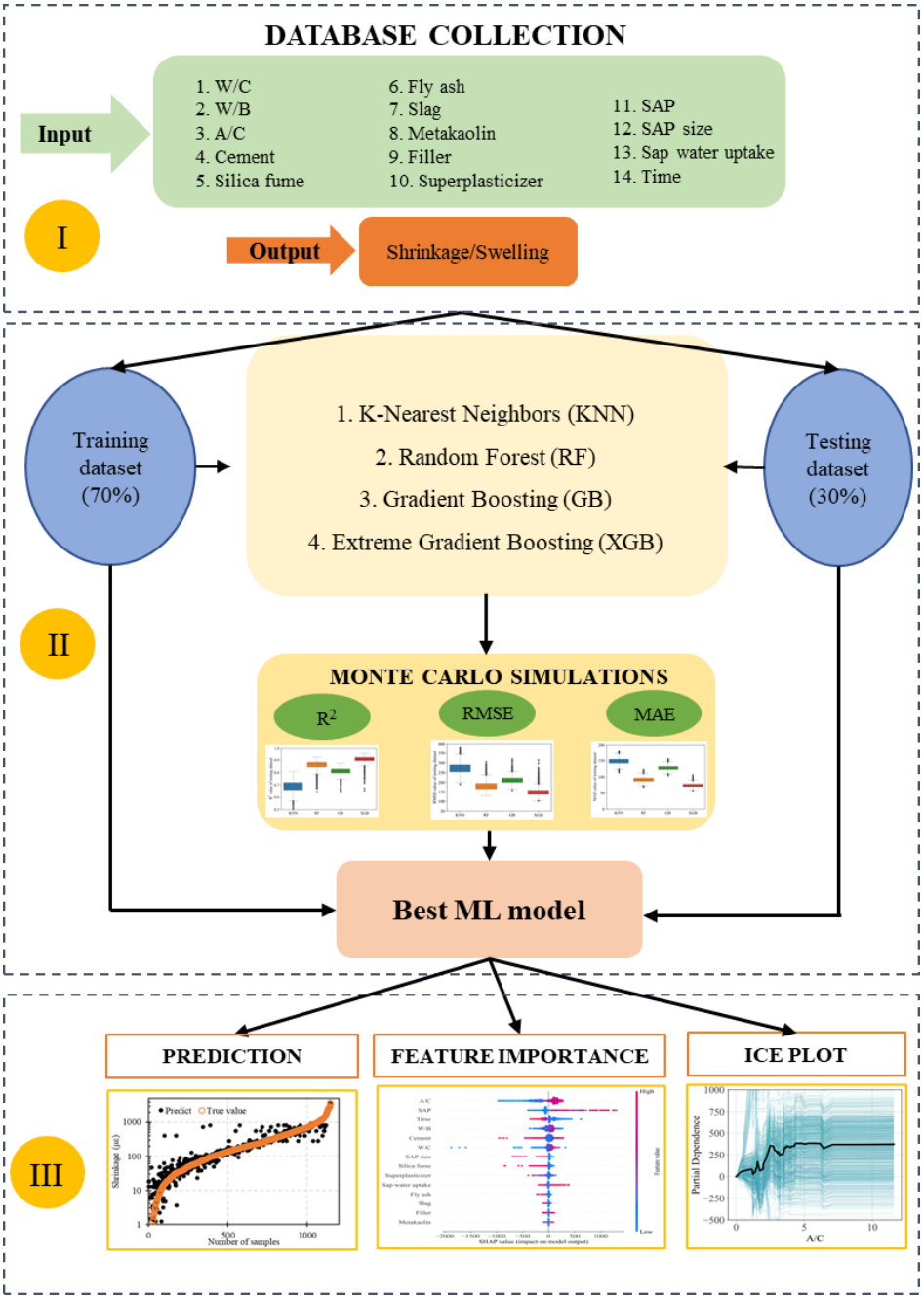

Fig 4. Conception of shrinkage/swelling investigation

4. Results and Discussion

4.1. Performance evaluation of machine learning models

The performance of the four models on the testing set has been evaluated using the metrics mentioned above for 3000 simulations varying the initial train-test split. Random Forest and XGBoost algorithms performed significantly better than Gradient Boosting and K-Nearest

Neighbors on the training and testing sets, as illustrated in Fig.5.

The generalization capacity of the models has been evaluated by predicting the shrinkage / swelling values of the 567 samples in the test set. Minor discrepancies were observed between the accuracy of the training set and the testing set. The extent of overfitting was measured as marginal and therefore has been reasonably neglected. As illustrated in Fig. 5, comparing the performance of the four models, RF and XGBoost obtained the best results on the test set during training. The mean values of the performance metrics of the four models have been reported in Table 2. Mean R^2 values of 0.958 and 0.971 were obtained on the training set using RF and XGBoost models resp. These values correspond to small RMSE values of 101 με and 84 με resp. Despite the limited data, mean performance metrics were good on the test data. Mean R^2 values of 0.859 and 0.904 were obtained on the test set using RF and XGBoost models resp. These values correspond to limited RMSE values of 183 με and 150 με resp.

The best prediction performance has been obtained using the XGBoost model. With this model, R^2 and RMSE values of 0.954 and 111.6 με have been obtained. These values are on par with other values reported for autogenous or drying shrinkage predictions reported in the literature [49,50] and calculated RMSE is consistent with the variability of shrinkage measurements obtained during a round Robin test [76].

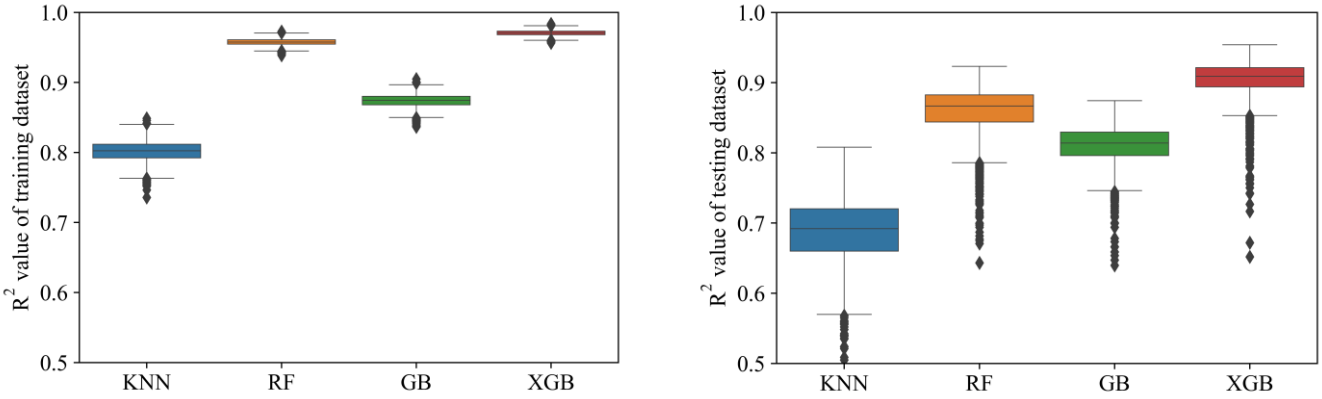

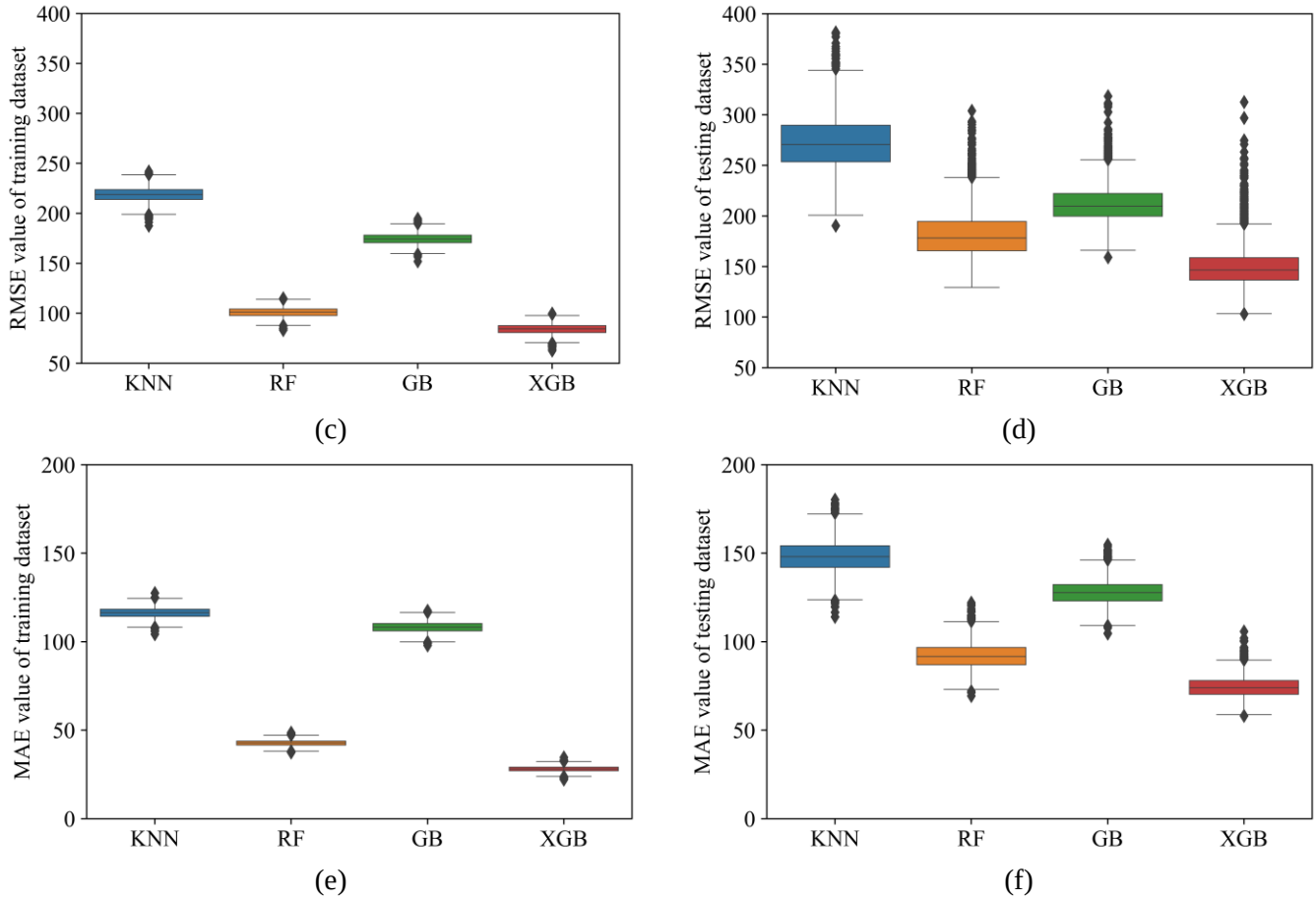

Fig. 5. Performance of machine learning models after 3000 simulations

Table 2. Comparison of machine learning algorithms for autogenous shrinkage/expansion prediction of concrete incorporating SAP using mean performance value

Algorithm	Training set			Test set		
	R^2	RMSE/με	MAE/με	R^2	RMSE/με	MAE/με
KNN	0.802	218.667	116.332	0.688	272.809	148.203
GB	0.874	174.378	108.200	0.811	212.455	127.898
XGB	**0.971**	**84.103**	**28.061**	**0.904**	**150.337**	**74.457**

4.2. Shrinkage/Swelling Prediction of typical machine learning model

The performance of a typical XGBoost model during training and testing is illustrated in Fig. 6 and 7. As illustrated in Fig. 6 a) and b), the model performed well on the training dataset for shrinkage and swelling. Only six data points over 175 (around 4 %) were misclassified as

shrinkage values while they were relatively small swelling values. As illustrated in Fig 6 b), the model correctly captured the shrinkage phenomenon, and only a few data points were not correctly predicted on the training set. The model predictions, illustrated in Fig. 6 c) and d) agreed with the measured values. As illustrated in Fig. 6 c), the model could correctly predict the swelling values higher than 100 με when SAP were included in the mix for 20 data points, and only relatively limited errors were produced on samples exhibiting swelling values close to 0 με. Shrinkage values, represented in Fig. 6 d), were predicted with very good precision for most of the samples in the test set. Only a small portion of predictions was found relatively far from the actual measured values: some shrinkage values were overestimated while actual values were smaller than 50 με.(top left part of the figure) while six predictions were clearly underestimated for actual measured values between 50 and 350 με.

The histograms of the errors between predicted and actual values are reported in Fig. 7. The errors were almost symmetric for both the train and the test sets. A small standard error was observed in the case of the training set, and a slightly larger standard error was made on the test set.

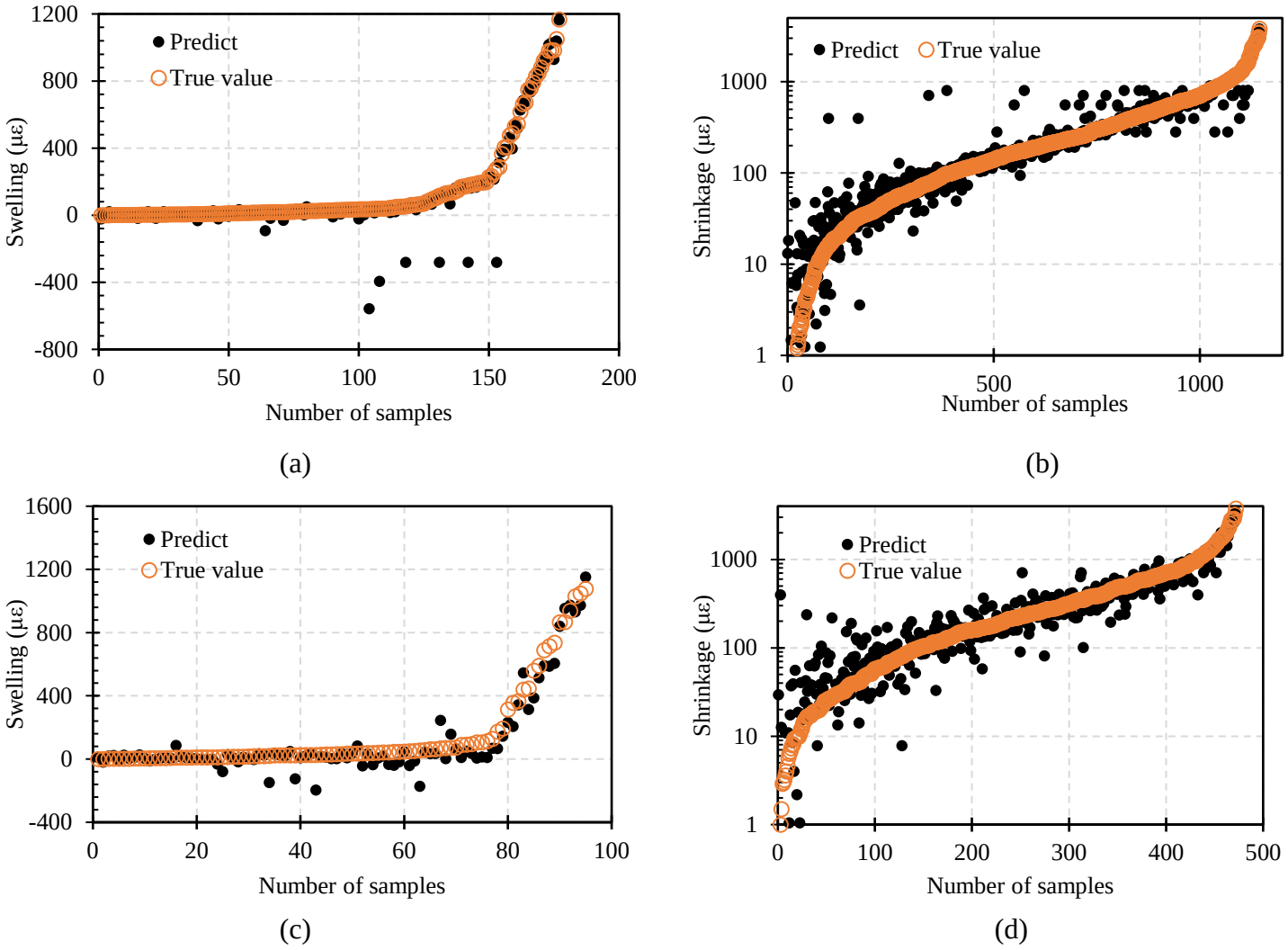

Fig. 6. Comparison between target and calculated outputs of typical XGB model for training and testing database

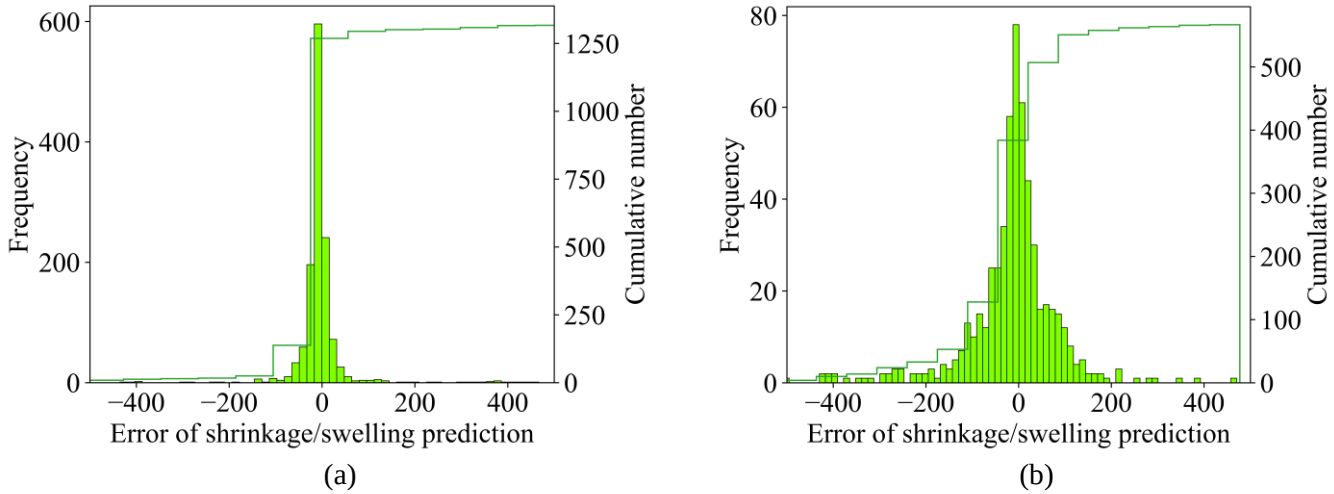

Fig. 7. Histograms of the error values between predicted and experimental shrinkage/expansion values for (a) training part, (b) testing part.

4.3. Feature importance analysis using Shapley Additive Explanations (SHAP)

In this study, the SHaple Additive exPlanation (SHAP) provides both local and global interpretations of each input parameter. SHAP provides comparable information to feature importance which has been largely used in the literature, but is more appropriate to ensemble machine learning models as it is more stable and provides quantitative information.

The SHAP values of each feature, sorted in order of their average SHAP value, are shown in Fig. 8. The features listed on top of the graphical representation can be associated with the larger contributions to the model outputs. The most influencing parameters on shrinkage predictions were the aggregate-to-cement ratio (A/C), the SAP content, time (days since the beginning of shrinkage measurements), water-to-binder ratio, cement content, water-to-cement ratio, SAP size, and silica fume content. A clear boundary can be observed for all these parameters between high and low feature values influence on the model output: high A/C ratio increases SHAP value, that is to say, decrease shrinkage; high SAP content decreases shrinkage and, most of the time, this was found to be the most influential parameter; high time values correspond to higher shrinkage values; high w/b and w/c tend to decrease shrinkage while high silica fume replacement ratio or cement content mostly induces higher shrinkage, and large SAP size decreases SAP beneficial effect and increases shrinkage compared to smaller SAP sizes. These influences are in agreement with experimental observations.

The less influencing parameters were identified: superplasticizer, fly ash, slag, filler, and calcined clay content. These observations based on the SHAP values are consistent with the experimental observations as these parameters are known to have a more negligeable influence on shrinkage than the ones mentioned above.

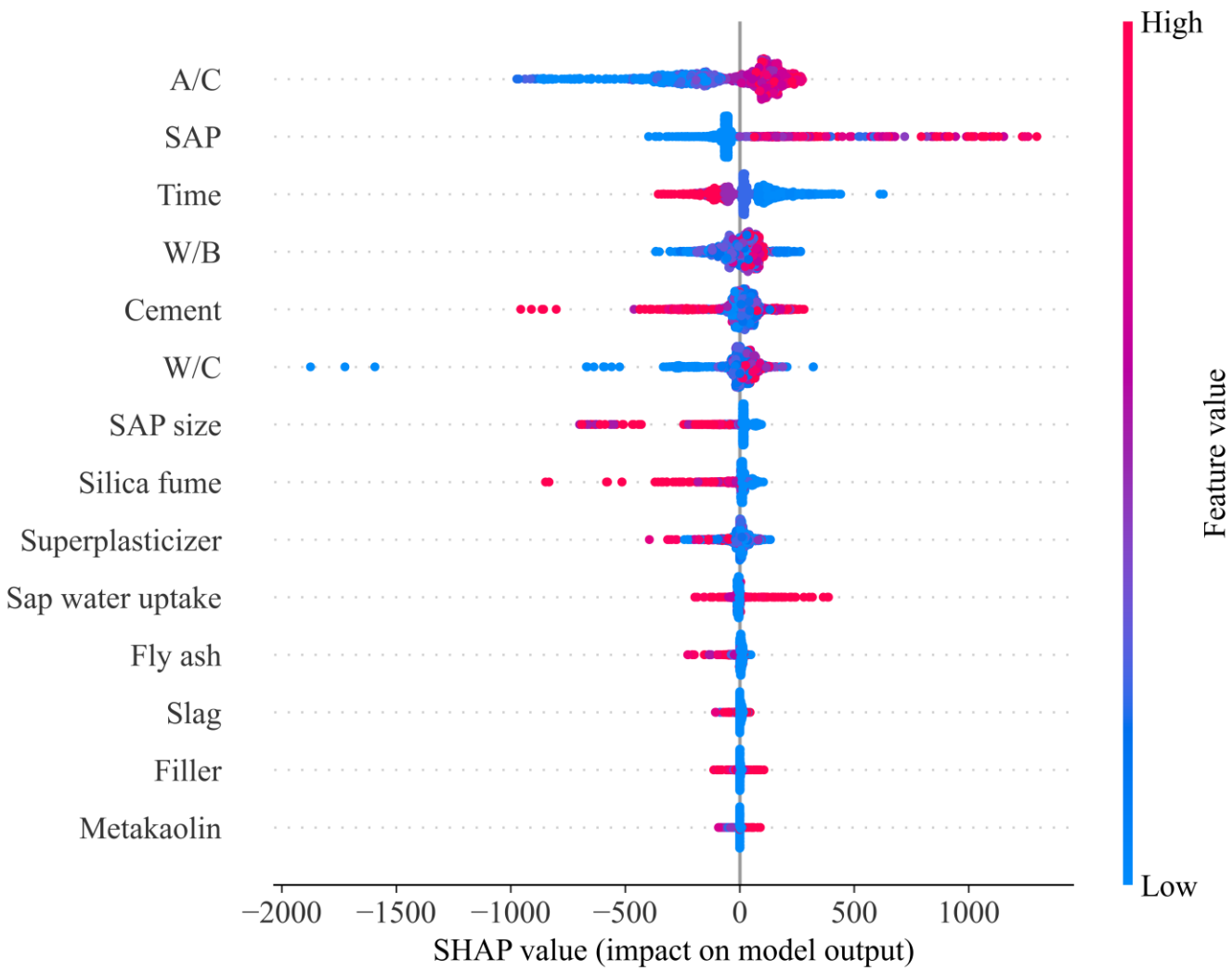

Fig.8. Feature importance analysis using the Shap library in Python code

4.4. Partial dependence plot analysis for shrinkage/swelling prediction

More information about the model predictions can be obtained using the partial difference plots, which represent the quantitative influence of any given parameter on the output. The partial difference plots of each parameter on the output are illustrated in Fig. 9, the most influencing parameters first. As illustrated in Fig 9 a), shrinkage gradually decreases with the increase of the A/C ratio for ratios between 0 and around 5. A mean shrinkage decrease of around 350 με was predicted by the model between A/C ratio of 0 and A/C ratio of 5 which corresponds to the transition from pure cement paste to normal concrete. Also, as illustrated in Fig. 9 b), SAP content also decreases shrinkage almost regularly between SAP content equal to 0 % of the cement mass and around 0.6 % of the cement mass. On average, shrinkage was reduced by around 300 με when

an amount of SAP equal to 0.6% of the cement mass was used compared to formulations without SAP. For SAP contents higher than 0.6 % of the cement mass, the model predicted a decrease of the partial dependence, highlighting a limited interest in including more SAP. SAP diameters higher than 100 µm were found to slightly decrease the beneficial impact of SAP as they were associated with partial dependence values around 200 µε smaller than smaller SAP sizes around 50-60 µm. No major influence of SAP water uptake could be detected using partial dependence plots, which can be attributed to the fact that the database only included positive published results, i.e., results with beneficial impact of SAP whatever their water uptake.

As expected, the partial dependence of shrinkage decreased with time, and the global trend is very similar to a shrinkage curve in all the cases (Fig. 9 c)). Water-to-binder and water-to-cement ratios particularly influence autogenous shrinkage for values smaller than 0.4 as illustrated in Fig 9 d) and f). On average, shrinkage was predicted 500 µε higher in the case of a water-to-binder ratio of 0.2 compared to a water-to-binder ratio of 0.4. Although the other parameters were not found as important by the model, partial dependence plots show that the model predicted increasing shrinkage values with increasing amounts of silica fume and slag (Fig 9 h), k) and l)) as commonly admitted in the literature but predicted an increase of shrinkage with fly ash content which is not in agreement. Contrarily to results reported in the literature, fly ash increased shrinkage on average. However, this result can be attributed to outliers associated with negative partial differences close to -400 µe that particularly influence the results even if most predictions were associated with no effect. Filler and calcined clay showed little influence, which is in relatively good agreement with the literature. The model would benefit from additional literature on these latest points, but studies dissociating the influence of fillers and calcined clay from the other SCM are scarce.

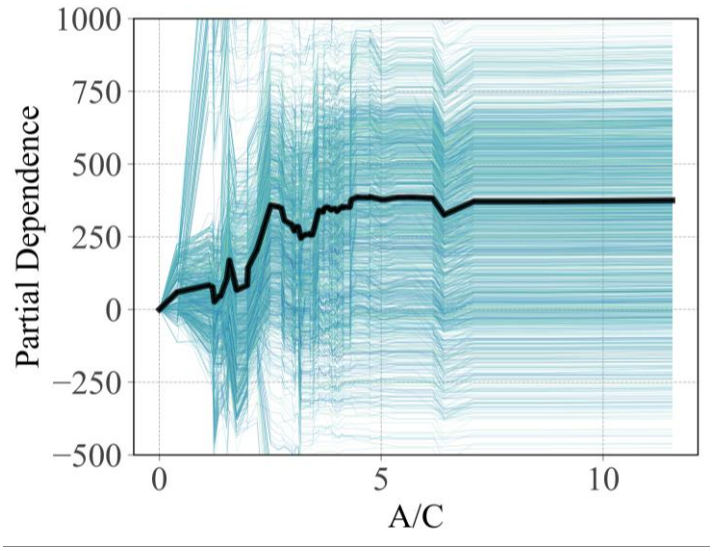
Partial Dependence
1000
750
500
250
0
−250
−500
0
5
10
A/C

(a)

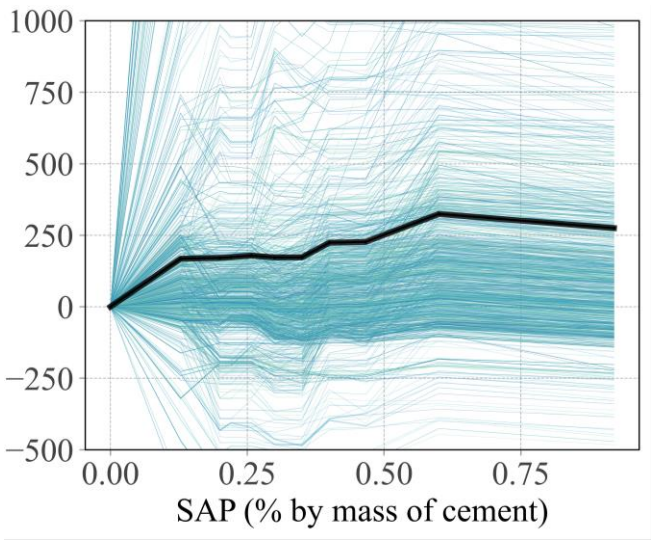
1000
750
500
250
0
−250
−500
0.00
0.25
0.50
0.75
SAP (% by mass of cement)

(b)

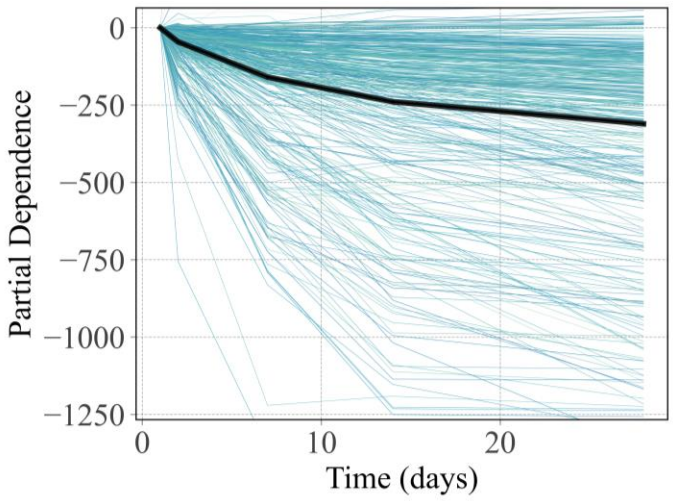
Partial Dependence
0
−250
−500
−750
−1000
−1250
0
10
20
Time (days)

(c)

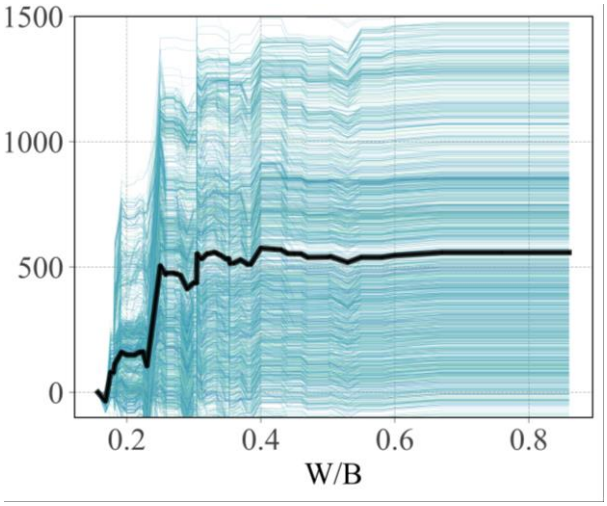
1500
1000
500
0
0.2
0.4
0.6
0.8
W/B

(d)

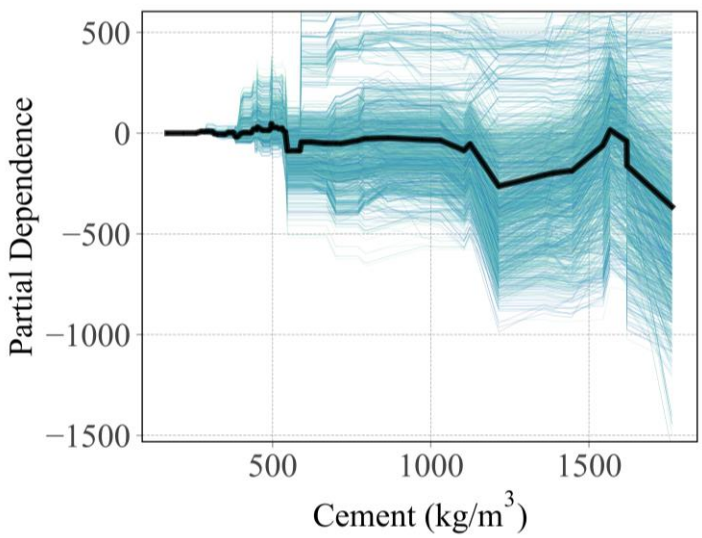
Partial Dependence
500
0
−500
−1000
−1500
500
1000
1500
Cement (kg/m3)

(e)

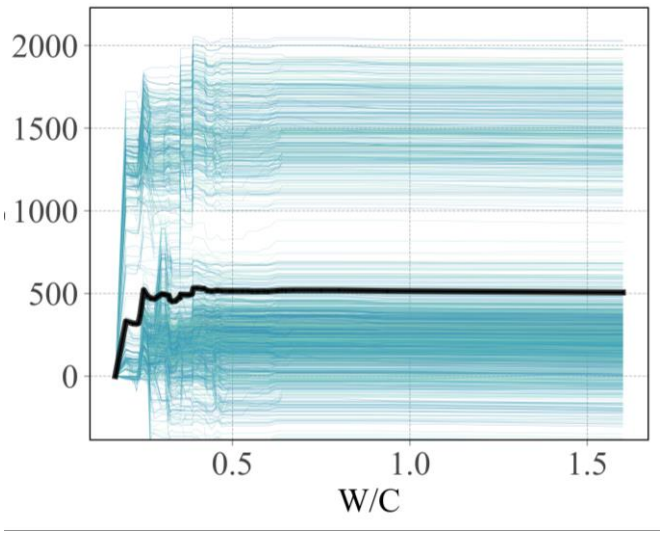
2000
1500
1000
500
0
0.5
1.0
1.5
W/C

(f)

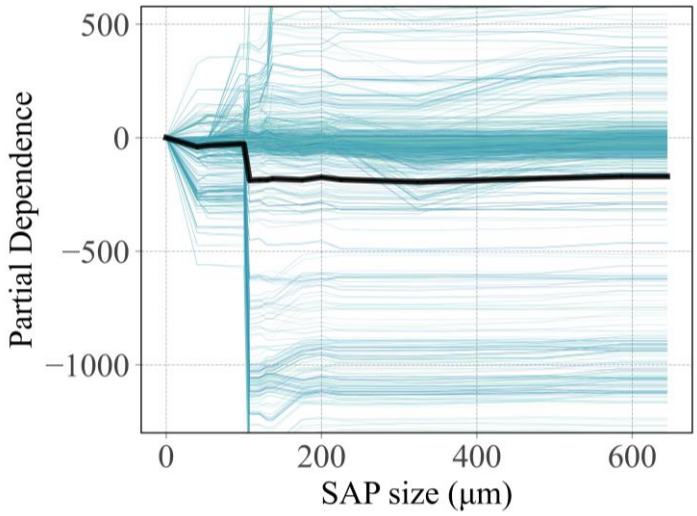
Partial Dependence
500
0
−500
−1000
0
200
400
600
SAP size (µm)

(g)

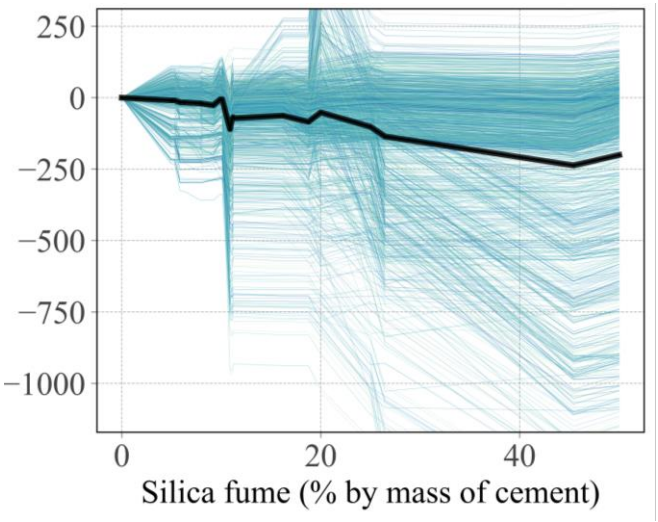
250
0
−250
−500
−750
−1000
0
20
40
Silica fume (% by mass of cement)

(h)

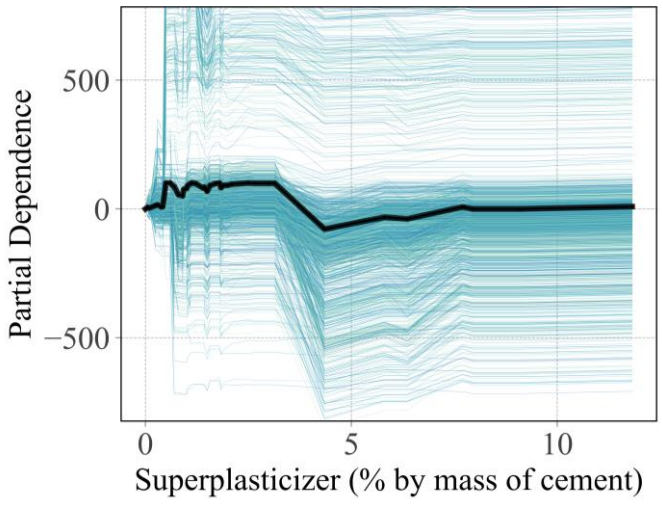
Partial Dependence
500
0
−500
0
5
10
Superplasticizer (% by mass of cement)

(i)

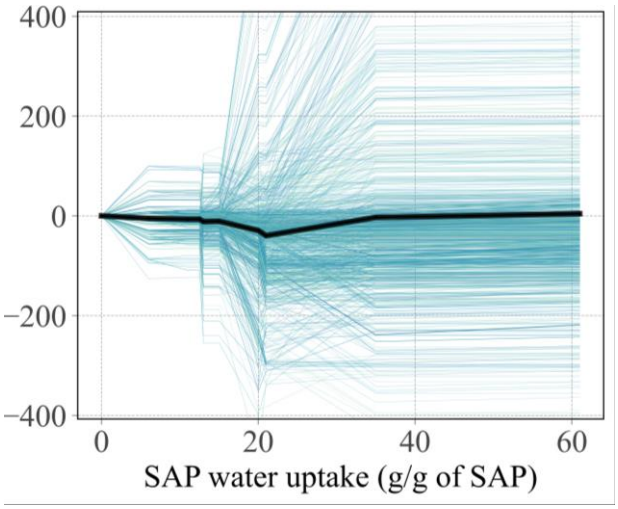
400
200
0
−200
−400
0
20
40
60
SAP water uptake (g/g of SAP)

(j)

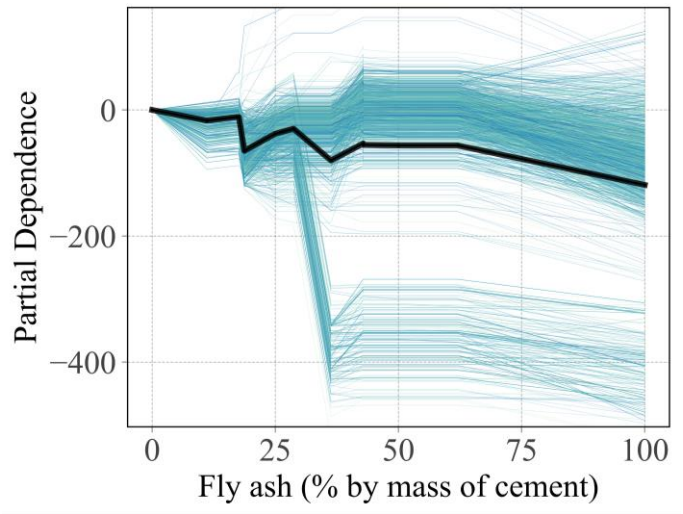
Partial Dependence
0
−200
−400
0
25
50
75
100
Fly ash (% by mass of cement)

(k)

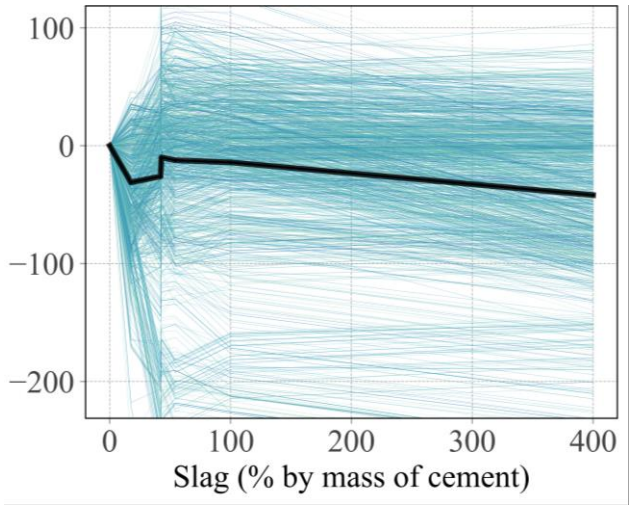
100
0
−100
−200
0
100
200
300
400
Slag (% by mass of cement)

(l)

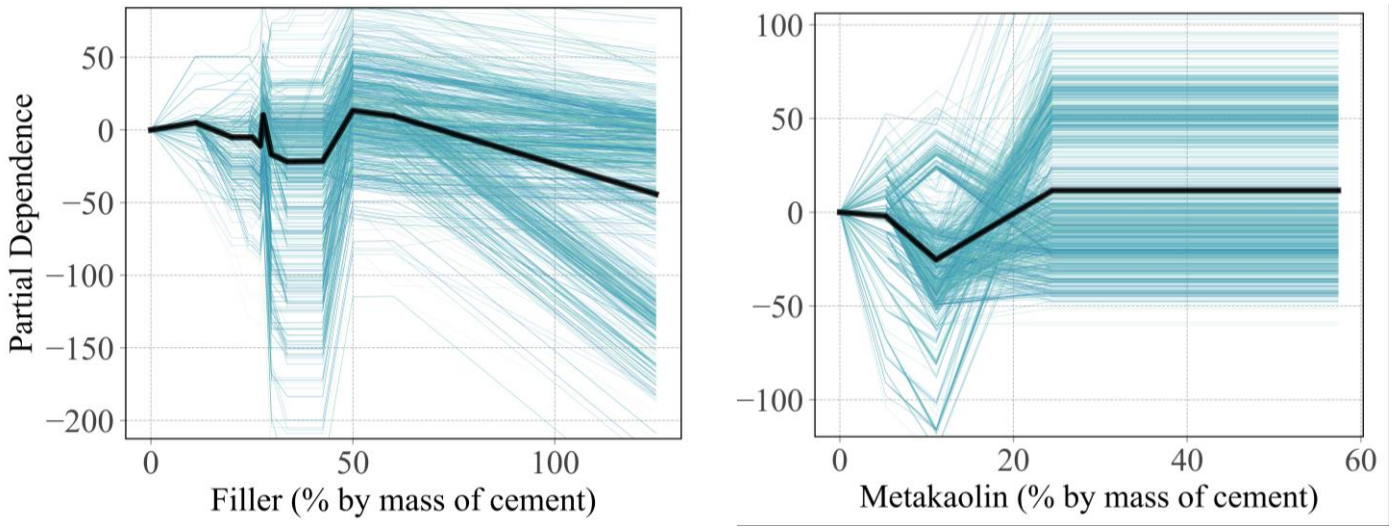

(m) (n)

Fig. 9. Partial dependence plots (PDP 1D) analysis of the input variables effect on shrinkage/swelling of cementitious materials

The results of PDP 1D can be used for the preliminary study of concrete mix designs as the quick estimation of shrinkage/swelling can be performed with the help of figure 9. Indeed, using the initial mix composition, each graph in figure 9 can give a shrinkage/swelling gain value due to one parameter. For example, Table 3 illustrates the autogenous shrinkage/swelling values prediction at 1 and 2 days for three concretes with constant w/c of 0.25 incorporating three SAP contents (0%, 0.35%, and 0.7%). A w/b ratio of 0.25 leads to a gain value of 158 µe. This value is calculated relative to the minimum w/b ratio in the database (0.157), associated with a null gain since the higher the w/b ratio, the smaller the shrinkage. The A/C ratio of 2.82 is associated with a gain value of 304 µe because mortars and concretes shrink significantly less than pure cement paste, and cement content of 582 kg/m^3 gain is equal to -67 µe . SAP parameters exhibit similar gains in amplitude, thus consistently affecting predicted shrinkage/swelling values. In the end, predicted shrinkage/swelling values can be obtained by adding the mean shrinkage value (at 1 day) that is -280.93 µe and all the gains.

Table 3. Application PDP 1D in predicting shrinkage/swelling of the concrete W/B=0.25

	True mix design						Gain value according PDP plot					
W/B	0.25	0.25	0.25	0.25	0.25	0.25	158	158	158	158	158	158
A/C	2.82	2.82	2.82	2.82	2.82	2.82	304	304	304	304	304	304
Cement content	582	582	582	582	582	582	-67	-67	-67	-67	-67	-67
Fly ash content	0	0	0	0	0	0	0	0	0	0	0	0
Slag content	0	0	0	0	0	0	0	0	0	0	0	0
Silica fume content	0	0	0	0	0	0	0	0	0	0	0	0
Metakaolin content	0	0	0	0	0	0	0	0	0	0	0	0
Filler content	0	0	0	0	0	0	0	0	0	0	0	0
Superplasticizer content	1.4	1.4	1.4	1.4	2	2	10	10	10	10	10	10
SAP content	0	0	0.35	0.35	0.7	0.7	0	0	172	172	310	310
SAP size	200	200	200	200	200	200	-200	-200	-200	-200	-200	-200
Sap water uptake	13	13	13	13	13	13	0	0	0	0	0	0
Time	1	2	1	2	1	2	0	-58	0	-58	0	-58
	True swelling/shrinkage						Predicted= mean value (-280.93) + $\sum Gain$					
Shrinkage/Swelling	-171	-189.6	-19.6	-40.1	23.1	23.1	*-75.9*	*-133.9*	*96.1*	*38.1*	*234.1*	*176.1*

5. Conclusions

This study investigated the potential of machine learning models to predict the autogenous shrinkage of cementitious materials incorporating supplementary cementitious materials (SCM) and superabsorbent polymers (SAP). A new database has been built by combining shrinkage results reported in NU database and available studies dealing with the influence of SCM and SAP on autogenous concrete. Four machine learning models have been built: K-nearest neighbors (KNN), Random Forest (RF), Gradient Boosting (GB), and Extreme Gradient Boosting (XGBoost). The machine learning model performances have been studied using Monte-Carlo simulation. Shapley Additives Explanations (SHAP) and partial dependence plots were then used to interpret the machine learning models' performance. The results have been discussed and compared to the available literature about autogenous shrinkage of cementitious materials with SCM and/or SAP. The following main conclusions can be drawn:

- A comprehensive database grouping 437 studies from the literature can be built (108 shrinkage results published in articles related to shrinkage of cementitious materials with SAP, 142 shrinkage results from studies related to the effect of SCM on autogenous shrinkage, and 187 shrinkage values from NU database) and autogenous shrinkage values at 1 d, 2 d, 7 d, 14 d, and 28 d can be interpolated to generate a database containing 1889 shrinkage values at different times with 14 parameters related to the concrete composition,

SAP content, SAP size and SAP water uptake. Specific attention has been devoted to selecting diverse binary, ternary and quaternary experimental results within a broad range of water-to-binder ratios.

- The machine learning models can achieve high training and testing accuracy on par with neural network results published in the literature for predicting autogenous or drying shrinkage.
- Two ensemble machine learning models, Random Forest (RF) and Extreme Gradient Boosting (XGBoost), outperformed the other two models under investigation. This agrees with previous machine learning models developed for cementitious materials.
- Through Monte Carlo simulation, the XGBoost model can achieve a high accuracy on the training and testing sets, resp. R^2=0.962 and 0.954. The predictions of machine learning models are in good agreement with the experimentally measured values for shrinkage/expansion values ranging from -3800 με (shrinkage) to around 1200 με (expansion). XGB algorithms with default hyperparameters are suitable for building soft computing tools in predicting the shrinkage/swelling of concrete containing SAP .
- The tuned models can be interpreted using SHAP values. The most influential parameters were aggregate-to-cement (A/C) ratio, SAP content, time, water-to-binder (w/b) ratio, water-to-cement ratio, cement content, and SAP size. The respective influences of these parameters are consistent with experimental observations.
- Partial difference plots highlighted the influence of the parameters on the predicted shrinkage values. It was found that shrinkage gradually decreases with increasing A/C and w/b ratios between 0 and 5 and 0.2 and 0.4 resp., and SAP inclusion continuously reduces shrinkage for content up to 0.6 % of cement mass.

The study might open up new research paths related to the optimal usage of SAP in cementitious materials with SCM. For example, the results can guide the selection of concretes constituents to decrease short-term autogenous shrinkage. Additions to the database are encouraged to collaboratively build a more extensive database, including chemical descriptions of SAP or shrinkage measurement methodology, for example. Possible developments can also be envisioned by coupling the results reported herein and mechanical properties predictions. Such advanced models might be of interest in the future regarding high or ultra-high performance eco-

friendly cementitious materials development.

CRediT authorship contribution statement

Benoit Hilloulin: Conceptualization, Methodology, Investigation, Formal analysis, Writing -original draft, Writing - review & editing, Validation.

Van Quan Tran: Conceptualization, Methodology, Software**,** Visualization**.** Writing -original draft, Writing - review & editing, Validation.

Conflict of Interest: The authors declare that there is no conflict of interest.

Funding: This research did not receive any specific grant from funding agencies in the public, commercial, or not-for-profit sectors.

Availability of data and material: Data is provided as supplementary data.

References

[1] O. Bernard, E. Brühwiler, Influence of autogenous shrinkage on early age behaviour of structural elements consisting of concretes of different ages, Materials and Structures. 35 (2002) 7. https://doi.org/10.1007/BF02483123.

[2] D.P. Bentz, O.M. Jensen, Mitigation strategies for autogenous shrinkage cracking, Cement and Concrete Composites. 26 (2004) 677–685. https://doi.org/10.1016/S0958-9465(03)00045-3.

[3] J. Kheir, A. Klausen, T.A. Hammer, L. De Meyst, B. Hilloulin, K. Van Tittelboom, A. Loukili, N. De Belie, Early age autogenous shrinkage cracking risk of an ultra-high performance concrete (UHPC) wall: Modelling and experimental results, Engineering Fracture Mechanics. 257 (2021) 108024. https://doi.org/10.1016/j.engfracmech.2021.108024.

[4] A. Loukili, A. Khelidj, P. Richard, Hydration kinetics, change of relative humidity, and autogenous shrinkage of ultra-high-strength concrete, Cement and Concrete Research. 29 (1999) 577–584. https://doi.org/10/dbch8h.

[5] Y. Akkaya, C. Ouyang, S.P. Shah, Effect of supplementary cementitious materials on shrinkage and crack development in concrete, Cement and Concrete Composites. 29 (2007) 117–123. https://doi.org/10.1016/j.cemconcomp.2006.10.003.

[6] L. Wu, N. Farzadnia, C. Shi, Z. Zhang, H. Wang, Autogenous shrinkage of high performance concrete: A review, Construction and Building Materials. 149 (2017) 62–75. https://doi.org/10.1016/j.conbuildmat.2017.05.064.

[7] S. Tang, D. Huang, Z. He, A review of autogenous shrinkage models of concrete, Journal of Building Engineering. 44 (2021) 103412. https://doi.org/10.1016/j.jobe.2021.103412.

[8] E. Holt, Contribution of mixture design to chemical and autogenous shrinkage of concrete at early ages, Cement and Concrete Research. 35 (2005) 464–472. https://doi.org/10.1016/j.cemconres.2004.05.009.

[9] O.M. Jensen, Hansen, Freiesleben, Autogenous Deformation and Change of the Relative Humidity in Silica Fume-Modified Cement Paste., ACI Materials Journal. 6 (1996).

[10] M.H. Zhang, C.T. Tam, M.P. Leow, Effect of water-to-cementitious materials ratio and silica fume on the

autogenous shrinkage of concrete, Cement and Concrete Research. 33 (2003) 1687–1694. https://doi.org/10.1016/S0008-8846(03)00149-2.
[11] K.M. Lee, H.K. Lee, S.H. Lee, G.Y. Kim, Autogenous shrinkage of concrete containing granulated blast-furnace slag, Cement and Concrete Research. 36 (2006) 1279–1285. https://doi.org/10.1016/j.cemconres.2006.01.005.
[12] A. Darquennes, S. Staquet, M.-P. Delplancke-Ogletree, B. Espion, Effect of autogenous deformation on the cracking risk of slag cement concretes, Cement and Concrete Composites. 33 (2011) 368–379. https://doi.org/10.1016/j.cemconcomp.2010.12.003.
[13] P. Termkhajornkit, T. Nawa, M. Nakai, T. Saito, Effect of fly ash on autogenous shrinkage, Cement and Concrete Research. 35 (2005) 473–482. https://doi.org/10.1016/j.cemconres.2004.07.010.
[14] J.M. Khatib, Performance of self-compacting concrete containing fly ash, Construction and Building Materials. 22 (2008) 1963–1971. https://doi.org/10.1016/j.conbuildmat.2007.07.011.
[15] P.J.P. Gleize, M. Cyr, G. Escadeillas, Effects of metakaolin on autogenous shrinkage of cement pastes, Cement and Concrete Composites. 29 (2007) 80–87. https://doi.org/10.1016/j.cemconcomp.2006.09.005.
[16] J.J. Brooks, M.A.M. Johari, Effect of metakaolin on creep and shrinkage of concrete, (2001) 8.
[17] B. Akcay, M.A. Tasdemir, Performance evaluation of silica fume and metakaolin with identical finenesses in self compacting and fiber reinforced concretes, Construction and Building Materials. 185 (2018) 436–444. https://doi.org/10.1016/j.conbuildmat.2018.07.061.
[18] M. Valcuende, E. Marco, C. Parra, P. Serna, Influence of limestone filler and viscosity-modifying admixture on the shrinkage of self-compacting concrete, Cement and Concrete Research. 42 (2012) 583–592. https://doi.org/10.1016/j.cemconres.2012.01.001.
[19] A. Alrifai, S. Aggoun, A. Kadri, S. Kenai, E. Kadri, Paste and mortar studies on the influence of mix design parameters on autogenous shrinkage of self-compacting concrete, Construction and Building Materials. 47 (2013) 969–976. https://doi.org/10.1016/j.conbuildmat.2013.05.024.
[20] M. Bouasker, N.E.H. Khalifa, P. Mounanga, N. Ben Kahla, Early-age deformation and autogenous cracking risk of slag–limestone filler-cement blended binders, Construction and Building Materials. 55 (2014) 158–167. https://doi.org/10.1016/j.conbuildmat.2014.01.037.
[21] Y. Dhandapani, T. Sakthivel, M. Santhanam, R. Gettu, R.G. Pillai, Mechanical properties and durability performance of concretes with Limestone Calcined Clay Cement (LC3), Cement and Concrete Research. 107 (2018) 136–151. https://doi.org/10.1016/j.cemconres.2018.02.005.
[22] S.H. Kang, Y. Jeong, K.H. Tan, J. Moon, High-volume use of limestone in ultra-high performance fiber-reinforced concrete for reducing cement content and autogenous shrinkage, Construction and Building Materials. 213 (2019) 292–305. https://doi.org/10.1016/j.conbuildmat.2019.04.091.
[23] B. Kucharczyková, D. Kocáb, P. Daněk, I. Terzijski, Cost-Effective High-Performance Concrete: Experimental Analysis on Shrinkage, Materials. 12 (2019) 2730. https://doi.org/10.3390/ma12172730.
[24] L. Yang, C. Shi, Z. Wu, Mitigation techniques for autogenous shrinkage of ultra-high-performance concrete – A review, Composites Part B: Engineering. 178 (2019) 107456. https://doi.org/10.1016/j.compositesb.2019.107456.
[25] K. Aghaee, K.H. Khayat, Effect of shrinkage-mitigating materials on performance of fiber-reinforced concrete – An overview, Construction and Building Materials. 305 (2021) 124586. https://doi.org/10.1016/j.conbuildmat.2021.124586.
[26] B. Akcay, M.A. Tasdemir, Effects of distribution of lightweight aggregates on internal curing of concrete, Cement and Concrete Composites. 32 (2010) 611–616. https://doi.org/10/fv944d.
[27] D. Snoeck, S. Steuperaert, K.V. Tittelboom, P. Dubruel, N.D. Belie, Visualization of water penetration in cementitious materials with superabsorbent polymers by means of neutron radiography, Cement and Concrete Research. 42 (2012) 1113–1121. https://doi.org/10/f35rxz.
[28] O.M. Jensen, P.F. Hansen, Water-entrained cement-based materials: II. Experimental observations, Cement and Concrete Research. 32 (2002) 973–978. https://doi.org/10/bp7q5f.
[29] D. Snoeck, O.M. Jensen, N. De Belie, The influence of superabsorbent polymers on the autogenous shrinkage properties of cement pastes with supplementary cementitious materials, Cement and Concrete Research. 74 (2015) 59–67. https://doi.org/10.1016/j.cemconres.2015.03.020.
[30] M. Wyrzykowski, S.-I. Igarashi, P. Lura, V. Mechtcherine, Recommendation of RILEM TC 260-RSC: using

superabsorbent polymers (SAP) to mitigate autogenous shrinkage, Mater Struct. 51 (2018) 135. https://doi.org/10.1617/s11527-018-1241-9.
[31] V. Mechtcherine, M. Wyrzykowski, C. Schröfl, D. Snoeck, P. Lura, N. De Belie, A. Mignon, S. Van Vlierberghe, A.J. Klemm, F.C.R. Almeida, J.R. Tenório Filho, W.P. Boshoff, H.-W. Reinhardt, S.-I. Igarashi, Application of super absorbent polymers (SAP) in concrete construction—update of RILEM state-of-the-art report, Mater Struct. 54 (2021) 80. https://doi.org/10.1617/s11527-021-01668-z.
[32] S.-H. Kang, S.-G. Hong, J. Moon, Shrinkage characteristics of heat-treated ultra-high performance concrete and its mitigation using superabsorbent polymer based internal curing method, Cement and Concrete Composites. 89 (2018) 130–138. https://doi.org/10.1016/j.cemconcomp.2018.03.003.
[33] D. Shen, H. Shi, X. Tang, Y. Ji, G. Jiang, Effect of internal curing with super absorbent polymers on residual stress development and stress relaxation in restrained concrete ring specimens, Construction and Building Materials. 120 (2016) 309–320. https://doi.org/10.1016/j.conbuildmat.2016.05.048.
[34] L. De Meyst, E. Mannekens, M. Araújo, D. Snoeck, K. Van Tittelboom, S. Van Vlierberghe, N. De Belie, Parameter Study of Superabsorbent Polymers (SAPs) for Use in Durable Concrete Structures, Materials. 12 (2019) 1541. https://doi.org/10.3390/ma12091541.
[35] S.-H. Kang, S.-G. Hong, J. Moon, Absorption kinetics of superabsorbent polymers (SAP) in various cement-based solutions, Cement and Concrete Research. 97 (2017) 73–83. https://doi.org/10.1016/j.cemconres.2017.03.009.
[36] D. Snoeck, C. Schröfl, V. Mechtcherine, Recommendation of RILEM TC 260-RSC: testing sorption by superabsorbent polymers (SAP) prior to implementation in cement-based materials, Mater Struct. 51 (2018) 116. https://doi.org/10.1617/s11527-018-1242-8.
[37] J. Fořt, P. Migas, R. Černý, Effect of Absorptivity of Superabsorbent Polymers on Design of Cement Mortars, Materials. 13 (2020) 5503. https://doi.org/10.3390/ma13235503.
[38] P. Zhong, M. Wyrzykowski, N. Toropovs, L. Li, J. Liu, P. Lura, Internal curing with superabsorbent polymers of different chemical structures, Cement and Concrete Research. 123 (2019) 105789. https://doi.org/10.1016/j.cemconres.2019.105789.
[39] P. Lura, Autogenous strain of cement pastes with superabsorbent polymers, in: International RILEM Conference on Volume Changes of Hardening Concrete: Testing and Mitigation, RILEM Publications, Lyngby, Denmark, 2006: pp. 57–65. https://doi.org/10.1617/2351580052.007.
[40] I.-C. Yeh, Modeling of strength of high-performance concrete using artificial neural networks, Cement and Concrete Research. 28 (1998) 1797–1808. https://doi.org/10.1016/S0008-8846(98)00165-3.
[41] M.-Y. Cheng, J.-S. Chou, A.F.V. Roy, Y.-W. Wu, High-performance Concrete Compressive Strength Prediction using Time-Weighted Evolutionary Fuzzy Support Vector Machines Inference Model, Automation in Construction. 28 (2012) 106–115. https://doi.org/10.1016/j.autcon.2012.07.004.
[42] J. Karthikeyan, A. Upadhyay, N.M. Bhandari, Artificial Neural Network for Predicting Creep and Shrinkage of High Performance Concrete, ACT. 6 (2008) 135–142. https://doi.org/10.3151/jact.6.135.
[43] L. Bal, F. Buyle-Bodin, Artificial neural network for predicting creep of concrete, Neural Comput & Applic. 25 (2014) 1359–1367. https://doi.org/10.1007/s00521-014-1623-z.
[44] M. Liang, Z. Chang, Z. Wan, Y. Gan, E. Schlangen, B. Šavija, Interpretable Ensemble-Machine-Learning models for predicting creep behavior of concrete, Cement and Concrete Composites. (2021) 104295. https://doi.org/10.1016/j.cemconcomp.2021.104295.
[45] Y.J. Cha, W. Choi, O. Büyüköztürk, Deep Learning-Based Crack Damage Detection Using Convolutional Neural Networks, Computer-Aided Civil and Infrastructure Engineering. 32 (2017) 361–378. https://doi.org/10.1111/mice.12263.
[46] R. Cai, T. Han, W. Liao, J. Huang, D. Li, A. Kumar, H. Ma, Prediction of surface chloride concentration of marine concrete using ensemble machine learning, Cement and Concrete Research. 136 (2020) 106164. https://doi.org/10.1016/j.cemconres.2020.106164.
[47] V.Q. Tran, H.Q. Do, Prediction of California Bearing Ratio (CBR) of Stabilized Expansive Soils with Agricultural and Industrial Waste Using Light Gradient Boosting Machine, (2021) 9.
[48] V.Q. Tran, Compressive Strength Prediction of Stabilized Dredged Sediments Using Artificial Neural Network, Advances in Civil Engineering. 2021 (2021) 1–8. https://doi.org/10.1155/2021/6656084.
[49] L. Bal, F. Buyle-Bodin, Artificial neural network for predicting drying shrinkage of concrete, Construction

and Building Materials. 38 (2013) 248–254. https://doi.org/10.1016/j.conbuildmat.2012.08.043.
[50] K. Mermerdaş, M.M. Arbili, Explicit formulation of drying and autogenous shrinkage of concretes with binary and ternary blends of silica fume and fly ash, Construction and Building Materials. 94 (2015) 371–379. https://doi.org/10.1016/j.conbuildmat.2015.07.074.
[51] J. Liu, K. Yan, X. Zhao, Y. Hu, Prediction of autogenous shrinkage of concretes by support vector machine, International Journal of Pavement Research and Technology. 9 (2016) 169–177. https://doi.org/10.1016/j.ijprt.2016.06.003.
[52] M.H. Hubler, R. Wendner, Z.P. Bažant, Comprehensive Database for Concrete Creep and Shrinkage: Analysis and Recommendations for Testing and Recording, ACI Materials Journal. 112 (2015). https://doi.org/10.14359/51687453.
[53] S. Igarashi, A. Bentur, K. Kovler, Autogenous shrinkage and induced restraining stresses in high-strength concretes, Cement and Concrete Research. 30 (2000) 1701–1707. https://doi.org/10.1016/S0008-8846(00)00399-9.
[54] M.-Y. Xuan, Y. Han, X.-Y. Wang, The Hydration, Mechanical, Autogenous Shrinkage, Durability, and Sustainability Properties of Cement–Limestone–Slag Ternary Composites, Sustainability. 13 (2021) 1881. https://doi.org/10.3390/su13041881.
[55] X. Zhang, Z. Liu, F. Wang, Autogenous shrinkage behavior of ultra-high performance concrete, Construction and Building Materials. 226 (2019) 459–468. https://doi.org/10.1016/j.conbuildmat.2019.07.177.
[56] Z. Wu, C. Shi, K.H. Khayat, Investigation of mechanical properties and shrinkage of ultra-high performance concrete: Influence of steel fiber content and shape, Composites Part B: Engineering. 174 (2019) 107021. https://doi.org/10.1016/j.compositesb.2019.107021.
[57] R. Yang, R. Yu, Z. Shui, X. Gao, J. Han, G. Lin, D. Qian, Z. Liu, Y. He, Environmental and economical friendly ultra-high performance-concrete incorporating appropriate quarry-stone powders, Journal of Cleaner Production. 260 (2020) 121112. https://doi.org/10.1016/j.jclepro.2020.121112.
[58] M. Ding, R. Yu, Y. Feng, S. Wang, F. Zhou, Z. Shui, X. Gao, Y. He, L. Chen, Possibility and advantages of producing an ultra-high performance concrete (UHPC) with ultra-low cement content, Construction and Building Materials. 273 (2021) 122023. https://doi.org/10.1016/j.conbuildmat.2020.122023.
[59] A. Bentur, S. Igarashi, K. Kovler, Prevention of autogenous shrinkage in high-strength concrete by internal curing using wet lightweight aggregates, Cement and Concrete Research. 31 (2001) 1587–1591. https://doi.org/10.1016/S0008-8846(01)00608-1.
[60] L. Maia, H. Figueiras, S. Nunes, M. Azenha, J. Figueiras, Influence of shrinkage reducing admixtures on distinct SCC mix compositions, Construction and Building Materials. 35 (2012) 304–312. https://doi.org/10.1016/j.conbuildmat.2012.02.033.
[61] X. Wang, R. Yu, Z. Shui, Q. Song, Z. Zhang, Mix design and characteristics evaluation of an eco-friendly Ultra-High Performance Concrete incorporating recycled coral based materials, Journal of Cleaner Production. 165 (2017) 70–80. https://doi.org/10.1016/j.jclepro.2017.07.096.
[62] B. Akcay, M.A. Tasdemir, Optimisation of using lightweight aggregates in mitigating autogenous deformation of concrete, Construction and Building Materials. 23 (2009) 353–363. https://doi.org/10.1016/j.conbuildmat.2007.11.015.
[63] Y. Lee, S.-T. Yi, M.-S. Kim, J.-K. Kim, Evaluation of a basic creep model with respect to autogenous shrinkage, Cement and Concrete Research. 36 (2006) 1268–1278. https://doi.org/10.1016/j.cemconres.2006.02.011.
[64] L. Guangcheng, X. Youjun, J. Zhengwu, Volume changes of very-high-performance cement-based composites, Magazine of Concrete Research. 58 (2006) 657–663. https://doi.org/10.1680/macr.2006.58.10.657.
[65] D. Cusson, T. Hoogeveen, Internal curing of high-performance concrete with pre-soaked fine lightweight aggregate for prevention of autogenous shrinkage cracking, Cement and Concrete Research. 38 (2008) 757–765. https://doi.org/10.1016/j.cemconres.2008.02.001.
[66] X. Gao, S. Kawashima, X. Liu, S.P. Shah, Influence of clays on the shrinkage and cracking tendency of SCC, Cement and Concrete Composites. 34 (2012) 478–485. https://doi.org/10.1016/j.cemconcomp.2012.01.002.
[67] A. Itim, K. Ezziane, E.-H. Kadri, Compressive strength and shrinkage of mortar containing various amounts of mineral additions, Construction and Building Materials. 25 (2011) 3603–3609.

https://doi.org/10.1016/j.conbuildmat.2011.03.055.
[68] A.M. Soliman, M.L. Nehdi, Effect of drying conditions on autogenous shrinkage in ultra-high performance concrete at early-age, Mater Struct. 44 (2011) 879–899. https://doi.org/10.1617/s11527-010-9670-0.
[69] C. Jiang, Y. Yang, Y. Wang, Y. Zhou, C. Ma, Autogenous shrinkage of high performance concrete containing mineral admixtures under different curing temperatures, Construction and Building Materials. 61 (2014) 260–269. https://doi.org/10.1016/j.conbuildmat.2014.03.023.
[70] S.W. Yoo, S.-J. Kwon, S.H. Jung, Analysis technique for autogenous shrinkage in high performance concrete with mineral and chemical admixtures, Construction and Building Materials. 34 (2012) 1–10. https://doi.org/10.1016/j.conbuildmat.2012.02.005.
[71] M. Wyrzykowski, Z. Hu, S. Ghourchian, K. Scrivener, P. Lura, Corrugated tube protocol for autogenous shrinkage measurements: review and statistical assessment, Mater Struct. 50 (2017) 57. https://doi.org/10.1617/s11527-016-0933-2.
[72] G.-Z. Zhang, X.-Y. Wang, Effect of Pre-Wetted Zeolite Sands on the Autogenous Shrinkage and Strength of Ultra-High-Performance Concrete, Materials. 13 (2020) 2356. https://doi.org/10.3390/ma13102356.
[73] N.C. Thang, N.V. Tuan, K.-H. Yang, Q.T. Phung, Effect of Zeolite on Shrinkage and Crack Resistance of High-Performance Cement-Based Concrete, Materials. 13 (2020) 3773. https://doi.org/10.3390/ma13173773.
[74] A. Loukili, D. Chopin, A. Khelidj, J.-Y. Le Touzo, A new approach to determine autogenous shrinkage of mortar at an early age considering temperature history, Cement and Concrete Research. 30 (2000) 915–922. https://doi.org/10.1016/S0008-8846(00)00241-6.
[75] J.H. Yeon, Restrained Stress Development in Hardening Mortar Internally Cured with Superabsorbent Polymers under Autogenous and Drying Conditions, Polymers. 13 (2021) 979. https://doi.org/10.3390/polym13060979.
[76] V. Mechtcherine, M. Gorges, C. Schroefl, A. Assmann, W. Brameshuber, A.B. Ribeiro, D. Cusson, J. Custódio, E.F. da Silva, K. Ichimiya, S. Igarashi, A. Klemm, K. Kovler, A.N. de Mendonça Lopes, P. Lura, V.T. Nguyen, H.-W. Reinhardt, R.D.T. Filho, J. Weiss, M. Wyrzykowski, G. Ye, S. Zhutovsky, Effect of internal curing by using superabsorbent polymers (SAP) on autogenous shrinkage and other properties of a high-performance fine-grained concrete: results of a RILEM round-robin test, Mater Struct. 47 (2014) 541–562. https://doi.org/10.1617/s11527-013-0078-5.
[77] A.M. Soliman, M.L. Nehdi, Effect of partially hydrated cementitious materials and superabsorbent polymer on early-age shrinkage of UHPC, Construction and Building Materials. 41 (2013) 270–275. https://doi.org/10.1016/j.conbuildmat.2012.12.008.
[78] J. Liu, N. Farzadnia, C. Shi, X. Ma, Effects of superabsorbent polymer on shrinkage properties of ultra-high strength concrete under drying condition, Construction and Building Materials. 215 (2019) 799–811. https://doi.org/10.1016/j.conbuildmat.2019.04.237.
[79] J. Liu, N. Farzadnia, K.H. Khayat, C. Shi, Effects of SAP characteristics on internal curing of UHPC matrix, Construction and Building Materials. 280 (2021) 122530. https://doi.org/10.1016/j.conbuildmat.2021.122530.
[80] D. Shen, C. Liu, Z. Feng, S. Zhu, C. Liang, Influence of ground granulated blast furnace slag on the early-age anti-cracking property of internally cured concrete, Construction and Building Materials. 223 (2019) 233–243. https://doi.org/10.1016/j.conbuildmat.2019.06.149.
[81] L. De Meyst, E. Mannekens, K. Van Tittelboom, N. De Belie, The influence of superabsorbent polymers (SAPs) on autogenous shrinkage in cement paste, mortar and concrete, Construction and Building Materials. 286 (2021) 122948. https://doi.org/10.1016/j.conbuildmat.2021.122948.
[82] J. Liu, N. Farzadnia, C. Shi, X. Ma, Shrinkage and strength development of UHSC incorporating a hybrid system of SAP and SRA, Cement and Concrete Composites. 97 (2019) 175–189. https://doi.org/10.1016/j.cemconcomp.2018.12.029.
[83] E.F. Silva, M.A.R. Manzano, A.N.M. Lopes, R.D.T. Filho, Effect of SAP on the autogenous shrinkage and compressive strength of high-strength fne-grained concrete, in: International RILEM Conference on Application of Superabsorbent Polymers and Other New Admixtures in Concrete Construction, Viktor Mechtcherine and Christof Schroefl, 2014: pp. 211–219.
[84] D. Shen, C. Wen, P. Zhu, Y. Wu, Y. Wu, Influence of Barchip fiber on early-age autogenous shrinkage of high-strength concrete internally cured with super absorbent polymers, Construction and Building Materials.

264 (2020) 119983. https://doi.org/10.1016/j.conbuildmat.2020.119983.
[85] J. Yang, L. Liu, Q. Liao, J. Wu, J. Li, L. Zhang, Effect of superabsorbent polymers on the drying and autogenous shrinkage properties of self-leveling mortar, Construction and Building Materials. 201 (2019) 401–407. https://doi.org/10.1016/j.conbuildmat.2018.12.197.
[86] D. Shen, J. Jiang, M. Zhang, P. Yao, G. Jiang, Tensile creep and cracking potential of high performance concrete internally cured with super absorbent polymers at early age, Construction and Building Materials. 165 (2018) 451–461. https://doi.org/10.1016/j.conbuildmat.2017.12.136.
[87] S. Igarashi, Experimental study on prevention of autogenous deformation by internal curing using super-absorbent polymer particles, in: International RILEM Conference on Volume Changes of Hardening Concrete: Testing and Mitigation, RILEM Publications, Lyngby, Denmark, 2006: pp. 77–86. https://doi.org/10.1617/2351580052.009.
[88] D.P. Bentz, P. Lura, J.W. Roberts, Mixture Proportioning for Internal Curing, Concrete International. 27 (2005) 35–40.
[89] F. Pedregosa, G. Varoquaux, A. Gramfort, V. Michel, B. Thirion, O. Grisel, M. Blondel, P. Prettenhofer, R. Weiss, V. Dubourg, J. Vanderplas, A. Passos, D. Cournapeau, M. Brucher, M. Perrot, E. Duchesnay, Scikit-learn: Machine Learning in Python, Journal of Machine Learning Research. 12 (2011) 2825–2830.
[90] E. Fix, J.L. Hodges, Discriminatory Analysis. Nonparametric Discrimination: Consistency Properties, International Statistical Review / Revue Internationale de Statistique. 57 (1989) 238–247. https://doi.org/10.2307/1403797.
[91] N.S. Altman, An Introduction to Kernel and Nearest-Neighbor Nonparametric Regression, The American Statistician. 46 (1992) 175–185. https://doi.org/10.1080/00031305.1992.10475879.
[92] S.-B. Roh, Y.S. Kim, and T.-C. Ahn, Lazy Learning for Nonparametric Locally Weighted Regression, International Journal of Fuzzy Logic and Intelligent Systems. 20 (2020) 145–155. https://doi.org/10.5391/IJFIS.2020.20.2.145.
[93] L. Breiman, Bagging predictors, Mach Learn. 24 (1996) 123–140. https://doi.org/10.1007/BF00058655.
[94] T.K. Ho, The random subspace method for constructing decision forests, IEEE Transactions on Pattern Analysis and Machine Intelligence. 20 (1998) 832–844. https://doi.org/10.1109/34.709601.
[95] A. Liaw, M. Wiener, Classification and Regression by randomForest, R News 23. 2 (2002) 18–21.
[96] J.H. Friedman, Greedy function approximation: A gradient boosting machine., The Annals of Statistics. 29 (2001) 1189–1232. https://doi.org/10.1214/aos/1013203451.
[97] Z. Wei, Y. Meng, W. Zhang, J. Peng, L. Meng, Downscaling SMAP soil moisture estimation with gradient boosting decision tree regression over the Tibetan Plateau, Remote Sensing of Environment. 225 (2019) 30–44. https://doi.org/10.1016/j.rse.2019.02.022.
[98] L. Liu, M. Ji, M. Buchroithner, Combining Partial Least Squares and the Gradient-Boosting Method for Soil Property Retrieval Using Visible Near-Infrared Shortwave Infrared Spectra, Remote Sensing. 9 (2017) 1299. https://doi.org/10.3390/rs9121299.
[99] T. Chen, C. Guestrin, XGBoost: A Scalable Tree Boosting System, in: Proceedings of the 22nd ACM SIGKDD International Conference on Knowledge Discovery and Data Mining, ACM, New York, NY, USA, 2016: pp. 785–794. https://doi.org/10.1145/2939672.2939785.
[100] A. Goldstein, A. Kapelner, J. Bleich, E. Pitkin, Peeking Inside the Black Box: Visualizing Statistical Learning with Plots of Individual Conditional Expectation, ArXiv:1309.6392 [Stat]. (2014). http://arxiv.org/abs/1309.6392 (accessed October 13, 2021).